



HAL
open science

Photochemical box modelling of volcanic SO₂ oxidation: isotopic constraints

Tommaso Galeazzo, Slimane Bekki, Erwan Martin, Joel Savarino, Stephen R. Arnold

► **To cite this version:**

Tommaso Galeazzo, Slimane Bekki, Erwan Martin, Joel Savarino, Stephen R. Arnold. Photochemical box modelling of volcanic SO₂ oxidation: isotopic constraints. *Atmospheric Chemistry and Physics*, 2018, 18 (24), pp.17909-17931. 10.5194/acp-18-17909-2018 . insu-01966512

HAL Id: insu-01966512

<https://insu.hal.science/insu-01966512v1>

Submitted on 28 Dec 2018

HAL is a multi-disciplinary open access archive for the deposit and dissemination of scientific research documents, whether they are published or not. The documents may come from teaching and research institutions in France or abroad, or from public or private research centers.

L'archive ouverte pluridisciplinaire **HAL**, est destinée au dépôt et à la diffusion de documents scientifiques de niveau recherche, publiés ou non, émanant des établissements d'enseignement et de recherche français ou étrangers, des laboratoires publics ou privés.



Photochemical box modelling of volcanic SO₂ oxidation: isotopic constraints

Tommaso Galeazzo^{1,2}, Slimane Bekki¹, Erwan Martin², Joël Savarino³, and Stephen R. Arnold⁴

¹LATMOS/IPSL, Sorbonne Université, UVSQ, Université Paris-Saclay, CNRS, Paris, France

²ISTeP, Sorbonne Université, CNRS, Paris, France

³IGE, Univ. Grenoble Alpes, CNRS, IRD, INP-G, 38000 Grenoble, France

⁴Institute for Climate and Atmospheric Science, School of Earth and Environment, University of Leeds, Leeds, UK

Correspondence: Tommaso Galeazzo (tommaso.galeazzo@gmail.com) and Slimane Bekki (slimane@latmos.ipsl.fr)

Received: 21 April 2018 – Discussion started: 26 April 2018

Revised: 6 October 2018 – Accepted: 12 October 2018 – Published: 18 December 2018

Abstract. The photochemical box model CiTtyCAT is used to analyse the absence of oxygen mass-independent anomalies (O-MIF) in volcanic sulfates produced in the troposphere. An aqueous sulfur oxidation module is implemented in the model and coupled to an oxygen isotopic scheme describing the transfer of O-MIF during the oxidation of SO₂ by OH in the gas-phase, and by H₂O₂, O₃ and O₂ catalysed by TMI in the liquid phase. Multiple model simulations are performed in order to explore the relative importance of the various oxidation pathways for a range of plausible conditions in volcanic plumes. Note that the chemical conditions prevailing in dense volcanic plumes are radically different from those prevailing in the surrounding background air. The first salient finding is that, according to model calculations, OH is expected to carry a very significant O-MIF in sulfur-rich volcanic plumes and, hence, that the volcanic sulfate produced in the gas phase would have a very significant positive isotopic enrichment. The second finding is that, although H₂O₂ is a major oxidant of SO₂ throughout the troposphere, it is very rapidly consumed in sulfur-rich volcanic plumes. As a result, H₂O₂ is found to be a minor oxidant for volcanic SO₂. According to the simulations, oxidation of SO₂ by O₃ is negligible because volcanic aqueous phases are too acidic. The model predictions of minor or negligible sulfur oxidation by H₂O₂ and O₃, two oxidants carrying large O-MIF, are consistent with the absence of O-MIF seen in most isotopic measurements of volcanic tropospheric sulfate. The third finding is that oxidation by O₂/TMI in volcanic plumes could be very substantial and, in some cases, dominant, notably because the rates of SO₂ oxidation by OH,

H₂O₂ and O₃ are vastly reduced in a volcanic plume compared to the background air. Only cases where sulfur oxidation by O₂/TMI is very dominant can explain the isotopic composition of volcanic tropospheric sulfate.

1 Introduction

Volcanic activity is one of the major natural forcers of the Earth's climate, as volcanic emissions alter the chemical composition and radiative properties of the atmosphere, at local, regional and even global scales (Stocker et al., 2013; Langmann, 2014). Beyond their environmental impacts, sulfuric acid aerosols have adverse effects on human health since they are linked to cardiovascular and respiratory diseases (Pope III, 2002; World Health Organization, 2009). Moreover, sulfate aerosols can lead to acid rain causing damage to vegetation and to urban infrastructures. Over the last decades, our understanding of volcanic emissions in the atmosphere has greatly improved, thanks to satellite and field measurements, and to more sophisticated physical-chemical models (Robock, 2000; Bobrowski et al., 2003; Mather et al., 2003; Textor et al., 2004; Roberts et al., 2009; von Glasow, 2010; Roberts et al., 2012, 2014). The main gases emitted to the atmosphere by volcanic activity are H₂O, CO₂, SO₂, H₂S and halogen species, such as HCl, HBr and HF (Textor et al., 2004; Rose et al., 2006; Oppenheimer et al., 2013). In addition, measurements at crater rims of volcanoes also suggest direct emissions of small amounts of sulfate aerosols (Allen et al., 2002; De Moor et al., 2013).

Among all the compounds emitted, volcanic sulfur gases and in particular SO₂, are considered to be the most effective in affecting climate. Climatic perturbations from volcanic emissions are principally caused by conversion of sulfur gases into sulfate aerosols, which can then interact with solar and terrestrial radiation via scattering and absorption (Stocker et al., 2013). Once injected into the troposphere, volcanic SO₂ is converted in few days typically to H₂SO₄ by a range of gas-phase and liquid-phase reactions taking place in volcanic plumes and clouds (Chin and Jacob, 1996; Stevenson et al., 2003a). In the atmosphere, depending on the oxidation pathway, H₂SO₄ is produced either in the gas phase or liquid phase. When generated in the gas-phase, volcanic H₂SO₄ condenses very rapidly onto pre-existing particles, or it may even form very small sulfate particles by nucleation. In the boundary layer, sulfate aerosols have a residence time much shorter than a week because of the fast wet and dry depositions. However, at higher altitudes, such as in the free troposphere, removal is much slower; consequently, volcanic sulfate aerosols can have a much longer residence time of up to a few weeks (Stevenson et al., 2003b, a; Kristiansen et al., 2016). In addition, the residence time of volcanic aerosols in the stratosphere can reach lifetimes of about a year (Thomason and Peter, 2006).

Nowadays, anthropogenic SO₂ emissions outweigh those from natural sources (Smith et al., 2011). Volcanic quiescent degassing and eruptions is an important natural source of SO₂, notably to the free troposphere (Bates et al., 1992; Graf et al., 1998). Volcanic emissions release about 10–13 Tg y⁻¹ of SO₂ to the atmosphere (Andres and Kasgnoc, 1998) and contribute to up to 10 % of total sulfur emissions to the atmosphere (Stevenson et al., 2003a). Remarkably, volcanic emissions also have a bigger impact on the tropospheric aerosol burden than other sulfur sources (Graf et al., 1998) because volcanoes tend to emit SO₂ at higher altitudes than most other surface sulfur emissions, where the lifetime is longer.

Most of the tropospheric sulfate is generated in the liquid phase (Alexander et al., 2009) via oxidation of aqueous SO₂ by dissolved oxidants of the atmosphere, such as H₂O₂, O₃, O₂ catalysed by transition metal ions (Fe(III) and Mn(II)) and, possibly, HOBr and HOCl (Vogt et al., 1996; von Glasow et al., 2002; Stevenson et al., 2003a; Berglen et al., 2004; Park et al., 2004; Alexander et al., 2009; von Glasow and Crutzen, 2013; Chen et al., 2016). Note that the importance of the halogen oxidation pathway remains unclear. A significant amount of tropospheric H₂SO₄ is formed in the gas phase via the termolecular reaction between SO₂ and hydroxyl radicals (OH) (Calvert et al., 1978). In presence of liquid water and for typical pH values of atmospheric water droplets (3.0 < pH < 5.6), SO₂ is quickly oxidized by dissolved H₂O₂, and the two species rarely coexist in liquid phases (Gervat et al., 1988; Chandler et al., 1988; Daum et al., 1990; Zuo and Hoigne, 1993; Laj et al., 1997). At acidic pH values, synergism among transition metal ions (TMI) enhances the rate of SO₂ oxidation by dissolved O₂

(Brandt et al., 1994; Brandt and van Eldik, 1995), which can thus compete with the other SO₂ oxidation channels. Particular attention has been paid recently to this heterogeneous oxidation pathway, since its contribution could have been underestimated in previous budget assessments of sulfate production in the troposphere (Alexander et al., 2009; Goto et al., 2011; Harris et al., 2013). During eruptive events, volcanoes emit large quantities of ash and coarse material rich in iron-minerals (mainly glass, and in lesser extents magnetite and hematite), which can easily dissolve in water because of the high acidity reached in volcanic cloud droplets and aerosols (Ayrís and Delmelle, 2012; Hoshyaripour et al., 2015; Maters et al., 2016). As a consequence, the O₂/TMI heterogeneous oxidation reaction may be more significant than previously thought.

Quantifying the importance of the different SO₂ oxidation pathways is challenging. It requires the quantification of, among other things, the rates of the different oxidation processes. Conventional methods rely mostly on models that are evaluated and constrained with atmospheric concentration measurements of oxidants, because there is no direct means of measuring chemical fluxes associated with individual reactions (Morin et al., 2008). Simultaneous measurements of SO₂ oxidants in both the gas- and liquid phases in the atmosphere, let alone specifically in a volcanic plume, would be experimentally challenging. Alternative approaches need to be considered to reduce the uncertainty in the relative contributions from the different oxidation pathways. Isotopic approaches can provide such constraints (Brenninkmeijer et al., 2003; Thiemens, 2006). Isotopic ratios, indeed, provide direct insights into the nature and importance of individual oxidation fluxes (Savarino et al., 2007; Morin et al., 2008; Martin et al., 2014).

Thanks to peculiar distribution of isotopes among its three oxygen atoms, ozone and its chemistry provides a useful tool of investigation for atmospheric processes using isotopic signatures. Ozone bears a very significant non-mass dependent (also called mass-independent) isotopic fractionation, which is due to its formation mechanism (Heidenreich III et al., 1986; Krankowsky et al., 1995; Marcus, 2013). Since oxygen atoms in tropospheric oxygen-bearing species sometimes originate directly or indirectly from ozone via multiple photochemical reactions, a variety of atmospheric species carry anomalous isotopic mass-independent fractionations (MIFs Thiemens, 2006). For oxygen-bearing species, the anomalous oxygen MIF ($\Delta^{17}\text{O}$, O-MIF) is calculated with respect to a reference standard:

$$\Delta^{17}\text{O} = \delta^{17}\text{O} - 0.52 \times \delta^{18}\text{O}. \quad (1)$$

Where $\delta^{17}\text{O}$ and $\delta^{18}\text{O}$ represent deviations to the reference standard isotopic ratios (R_{std}):

$$R_x = \frac{x\text{O}}{16\text{O}} \quad x = 17; 18, \quad (2)$$

and

$$\delta^x\text{O} = \frac{R_x}{R_{\text{std}}} - 1. \quad (3)$$

Ozone is a key chemical reactive species of the troposphere. Its isotopic anomaly is intrinsically generated (through photolysis and recombination reactions) instead of being inherited by isotopes transfer like for most atmospheric species (Marcus, 2013). Other oxygen-bearing species in the atmosphere can gain excess-¹⁷O by transfer of this ozone anomaly via reactions with ozone itself, reactions with species that have already inherited the ozone anomaly or via anomalous kinetic isotopic effect (Röckmann, 1998; Lyons, 2001; Michalski et al., 2003). As a consequence, transfer of oxygen MIF among atmospheric species is process-specific and can be used as a signature to trace the chemistry of species as they react with specific oxidants. Once the isotopic anomalies of the oxidants are characterized, the resulting $\Delta^{17}\text{O}$ of an end-oxidation product is simply a linear combination of the isotopic signatures of all the oxidation channels weighted by their respective contributions, to the total production of the end-oxidation products. During the last decade, there has been an increasing number of studies that have used O-MIF oxygen anomalies in oxidation products to constrain oxidation channels, often coupling isotopic measurements and photochemical isotopic modelling (Michalski et al., 2003; Alexander et al., 2005; Morin et al., 2008; Gromov et al., 2010; Michalski and Xu, 2010).

The isotopic signature in sulfates generated in the troposphere, the so-called secondary sulfate (by opposition to sulfate directly emitted in the atmosphere, the so-called primary sulfate) reflects the competition within different oxidation channels. In the liquid phase, sulfate oxygen MIF is produced during sulfur oxidation by transfer of isotopic anomalies from ozone and H₂O₂, whereas sulfate with O-MIF very close to 0‰ is produced in the liquid phase via O₂/TMI oxidation (i.e. -0.08‰). Mass-dependent (MIF anomaly = 0‰) sulfate is generally produced via OH oxidation in the gas-phase (Savarino and Thiemens, 1999a, b; Savarino et al., 2000; Martin et al., 2014).

Most present-day tropospheric sulfates have O-MIF anomalies ($\Delta^{17}\text{O}$), typically of the order of 1‰ (Lee et al., 2001; Lee and Thiemens, 2001). However, there is some variability. For instance, O-MIF of sulfate aerosols generated in marine environments are higher compared to isotopic anomalies found in continental sulfates (Alexander et al., 2005). Very significant $\Delta^{17}\text{O}$ have also been found in volcanic sulfates collected from ash deposits dating back to the Miocene and the Oligocene, whose values reach 3.5‰–5.8‰. These peculiar isotopic anomalies have been linked to a different oxidative state of the atmosphere at that time (Bao et al., 2000, 2003). Tropospheric volcanic sulfates of the present era distinguish themselves from other tropospheric sulfates by having a $\Delta^{17}\text{O}$ often close to 0 (within the measurement error of about 0.1‰). This feature is found all over

the world in sulfates collected from volcanic ashes of small and medium-size tropospheric explosive eruptions, independent of location or geology of ash deposits (Bao et al., 2003; Bindeman et al., 2007; Martin et al., 2014) (see Table 1). Notably, this is often the case for volcanic sulfate extracted from ash deposits which are found very far from volcanoes, where secondary sulfate is expected to dominate. The only exception is volcanic sulfates in ice cores originating from very large volcanic eruptions. This sulfate had formed and transited through the stratosphere (Savarino et al., 2003; Baroni et al., 2007).

The question is why tropospheric volcanic sulfate from volcanic ash deposits does not appear to carry some isotopic O-MIF as is the case for other types of tropospheric sulfates. One might expect part of sulfate produced by tropospheric oxidation of volcanic SO₂ to carry some MIF isotopic anomaly because the dominant SO₂ oxidants in the troposphere are thought to be species carrying O-MIFs (O₃ and H₂O₂) with some contribution from O₂/TMI (Martin et al., 2014). An important difference between volcanic sulfur and most other sources of sulfur is that it is often emitted within dense volcanic plumes whose chemical compositions are radically different from the background air. The purpose of the present box-modelling study is to explore in detail the oxidation and fate of volcanic sulfur in dense volcanic clouds and the resulting isotopic MIF signature in volcanic sulfate. The objective is to see to what extent the chemical environment of dense volcanic plumes may affect sulfur dynamics and pathways of oxidation and, hence, sulfate isotopic composition. The focus here is on volcanic clouds that are rich in sulfur but poor in halogens, such in the case of intra-plate and rifting plate volcanoes (e.g. Nyarogongo in Congo, Erta'ale in Ethiopia, Kīlauea in Hawai'i) (Aiuppa, 2009; Oppenheimer et al., 2013). Volcanic eruptions with remarkable low halogens to sulfur emissions are the Holuhraun (Bárðarbunga) eruption of 2012–2014 in Iceland (Ilyinskaya et al., 2017; Stefánsson et al., 2017), and the Kīlauea eruption of 2008 in Hawai'i (Mather et al., 2012). In particular, HCl/SO₂ ratios of the order of 10⁻² have been observed for the Kīlauea eruption of 2008 (i.e. HCl ≈ 10–50 ppbv).

The second section of this work describes the photochemical model, including its sulfur heterogeneous chemistry scheme and the associated oxygen isotopic scheme. The mass balance equations used to evaluate the transfer of MIF oxygen anomaly from ozone to volcanic sulfate via different oxidation pathways are also presented. The third section is devoted to the study of individual and combined oxidation pathways and the resulting isotopic signatures in numerical experiments for this work standard volcanic plume conditions. The fourth section covers sensitivity model studies, investigating how different parameters in volcanic plumes affect the final isotopic anomaly in sulfate. Dominant oxidation pathways are identified and the ability of the model to reproduce observed isotopic signatures of volcanic sulfate is assessed.

Table 1. Oxygen isotopic composition of volcanic sulfates from different tropospheric emissions of the present geological era.

Volcano & date of eruption	Sample distance (km)	Source	$\Delta^{17}\text{O}$ (‰)	Reference
Popocatepetl (Mexico), 2008	25	ash	0.35	Martin et al. (2014)
Spurr (Alaska, USA), 1992	265	ash	−0.14	Martin et al. (2014)
Fuego (Guatemala), 1974	57	ash	−0.04	Martin et al. (2014)
Negro Cerro (Nicaragua), 1947	12	ash	−0.06	Martin et al. (2014)
Parícutin (Mexico), 1948	5	ash	0.13	Martin et al. (2014)
Mt. St. Helens (USA), 1980	400	ash	0.02	Martin et al. (2014)
Gjálp (Iceland), 1998	< 30	ash	−0.07	Martin et al. (2014)
Pinatubo (Philippines), 1991	< 50	ash	−0.04	Bindeman et al. (2007)
Pinatubo (Philippines), 1991	< 50	ash	0.19	Bindeman et al. (2007)
Spurr (USA), 1953	n.a.	ash	0.06	Bindeman et al. (2007)
Vesuvius (Italy), 1872	n.a.	ash	−0.07	Bao et al. (2003)
Popocatepetl (Mexico), 1997	n.a.	ash	−0.08	Bao et al. (2003)
Spurr (USA), 1992	n.a.	ash	0.06	Bao et al. (2003)
Fuego (Guatemala), 1974	55	ash	−0.03	Bao et al. (2003)
Pinatubo (Philippines), 1991	n.a.	anhydrite from pumice	−0.01	Bao et al. (2003)
Santorini (Greece), Minoan age	n.a.	pumice + ash	0.09	Bao et al. (2003)
Masaya (Nicaragua), 2003	0	aerosols	0.1	Mather et al. (2006)
Masaya (Nicaragua), 2003	0	aerosols	0.2	Mather et al. (2006)

* Refer to Martin (2018) for a more extensive description regarding oxygen isotopic anomalies measured in tropospheric volcanic sulfate of present and past geological eras.

2 Modelling approach

The photochemical box model used during simulation is the Cambridge Tropospheric Trajectory model of Chemistry and Transport (CiTTYCAT), a photochemical box model developed to simulate tropospheric chemistry (Evans et al., 2000; Sander et al., 2006; Real et al., 2007; Pugh et al., 2012). It describes the standard gas-phase photochemistry accounting for kinetics of tropospheric species (bimolecular, termolecular and photodissociation reactions), and deposition of gases and particles. Photolysis reaction rates are evaluated using the Fast-J code (Wild et al., 2000). Kinetic data are taken from JPL's data sheets (Sander et al., 2006). CiTTYCAT had already been used with success to constrain seasonal pathways of reactive nitrogen species in the troposphere, through the implementation of its chemical scheme with an isotopic transfer scheme accounting for $\Delta^{17}\text{O}$ production in nitrates (Morin et al., 2008). We have extended the capabilities of the model by including parameterizations of the transfer of soluble species between liquid and gas phases, of SO₂ heterogeneous chemistry, of pH in the liquid phase and of MIF of oxygen atoms in sulfates.

2.1 General continuity equations

The model resolves differential coupled mass balance equations (continuity equations) describing the time evolution of species concentrations in the troposphere. For given initial (e.g. initial concentrations of species) and environmental conditions (e.g. pressure, temperature), mass balance equa-

tions are solved for each species, accounting for production and loss as follows:

$$\frac{dC_i}{dt} = P_i - L_i, \quad (4)$$

where C_i is the concentration of species i , P_i the sum of physical and chemical production rates for i , and L_i the sum of the physical and chemical loss rates of i .

Production and loss terms are calculated using chemical reaction kinetics, where time evolution of concentrations of chemical species depends on the relevant rate constants (k_i) and on concentrations of reactants. They also include liquid–gas transfer and deposition. In addition, mixing of air between the volcanic sulfur cloud and the outside background air is also accounted for. It is parameterized by a simple linear relaxation scheme resulting in an exponential decay of plume concentrations towards background concentrations (Methven et al., 2006; Arnold et al., 2007).

$$\left(\frac{dC_i}{dt}\right)_{\text{mixing}} = K_{\text{mix}} \times (C_i - C_{i(\text{bck.})}), \quad (5)$$

where K_{mix} is a first-order mixing rate coefficient representing all the processes mixing volcanic air with the background atmosphere and $C_{i(\text{bck.})}$ is the concentration of species i in the background air. K_{mix} is set to 0.1 d^{−1}, a value typical of low mixing in the free troposphere and corresponding to a characteristic mixing timescale of 10 days (Methven et al., 2006; Arnold et al., 2007).

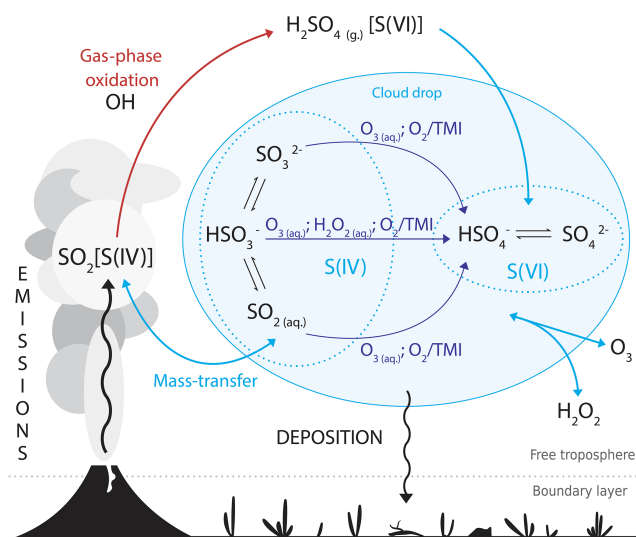


Figure 1. Diagram of the new sulfur scheme implemented in CiTTyCAT.

2.2 Liquid–gas mass transfer

Concentrations of relevant soluble species are calculated taking into account its partition between the gas and liquid phases. The transfer in both directions (evaporation, condensation) is dynamically computed. At each time step, rates of transfer are defined as follows:

$$\frac{d[C_{(\text{aq.})}]}{dt} = J_i \times (C_{(i)} - C_{(i,s)}), \quad (6)$$

where $C_{(i)}$ is gaseous concentration of species i far from liquid droplets, $C_{(i,s)}$ is the gaseous concentration of species i at the surface of droplets (which is assumed to be the equilibrium saturation vapour of i over the liquid) and J_i is the coefficient of condensation (from gas phase to liquid droplet) for species i , which is calculated using the Dahneke's expression (Dahneke, 1983) to cover mass-transfer from the continuum to the kinetic regime (see pg. 502 of Seinfeld and Pandis, 2016).

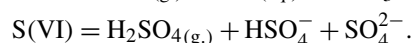
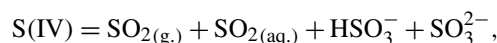
Throughout all the model simulations, droplets are assumed to be very large, with a radius of 5.0 μm . The sensitivity of the results to the assumed amount of liquid phase is explored varying the concentration of water droplets (and hence the liquid water content) instead of varying the size of droplets. It is also possible that emitted water condenses onto ash particles. Our treatment does not discriminate between liquid droplets and liquid phases at the surface of solid particles.

2.3 Gaseous and heterogeneous sulfur chemistry

The model already describes the SO₂ gas-phase chemistry. Since SO₂ is a mildly soluble species undergoing acid-base equilibrium in the liquid phase, we have added the gas-liquid

transfer and the chemical reactions and equilibrium associated with its presence in the liquid phase (see Table 2). The extent of SO₂ dissolution into water droplets is controlled by the pH. The oxidation of S(IV) species (HSO₃⁻, SO₃²⁻, SO_{2(aq.)}) by reactions with H₂O₂, O₃ or O₂ in the liquid phase pushes the gas-liquid partition towards dissolution of gaseous SO₂. A diagram of the sulfur chemical model is presented in Fig. 1. Since the model CiTTyCAT resolves continuity equations for species with gas-phase concentration units, liquid phase concentrations (e.g. M) and rate constants have to be expressed into gas-phase units in the code in order to be treated by the CiTTyCAT chemistry solver (Seinfeld and Pandis, 2016).

The species involved in the acid-base equilibriums of SO₂ and H₂SO₄ are often grouped together according to their oxidation state:



In these equations, dissolved H₂SO₄ is assumed to be totally dissociated. Ultimately, S(VI) in droplets ends up deposited at the Earth's surface. In the model, the amount of sulfate deposited is evaluated as a variable. The pH of volcanic water droplets is also a prognostic variable because sulfur species reaction rates and partitioning are pH dependent (Seinfeld and Pandis, 2016). It is dynamically calculated considering the most significant species dissolved in droplets:

$$= [\text{HSO}_3^-] + 2 \times [\text{SO}_3^{2-}] + [\text{HSO}_4^-] + 2 \times [\text{SO}_4^{2-}]. \quad (\text{R1})$$

The main aqueous equilibrium reactions and S(IV) oxidation reactions added to the chemical scheme are summarized in Table 3. The final continuity equation for single SO₂ oxidation channels can be expressed as follows:

$$-\frac{d[\text{SO}_2]}{dt} = k_{\text{OH}+\text{SO}_2} \times [\text{SO}_2][\text{OH}] + \sum_j (k_j \times [\text{S(IV)}]_{\text{aq.}} [C_j]_{\text{aq.}}), \quad (7)$$

where $k_{\text{OH}+\text{SO}_2}$ is the rate constant of the gas-phase reaction between OH and SO₂ (Sander et al., 2006), k_j the rate constant of the aqueous reaction between SO₂ and species C_j , whose concentration in the aqueous phase is expressed as $[C_j]_{\text{aq.}}$.

Similar continuity equations can easily be derived for all the sulfur species. The continuity equation for atmospheric sulfate S(IV) can be determined by summing all the individ-

Table 2. Sulfur aqueous equilibria.

Equilibrium	K (M ⁻¹),	$k_{298(\text{forward})}$ (M ⁻¹ s ⁻¹),	E_a/R (K),	$k_{298(\text{backward})}$ (M ⁻² s ⁻¹),
SO _{2(aq.)} + H ₂ O ⇌ HSO ₃ ⁻ + H ₃ O ⁺	3.13 × 10 ⁻⁴	6.27 × 10 ⁴	-1940	2 × 10 ^{8a,c}
HSO ₃ ⁻ + H ₂ O ⇌ SO ₃ ²⁻ + H ₃ O ⁺	6.22 × 10 ⁻⁸	3110	-1960	5 × 10 ^{10a,c}
H ₂ SO ₄ + H ₂ O → HSO ₄ ⁻ + H ₃ O ⁺		∞		
HSO ₄ ⁻ + H ₂ O ⇌ SO ₄ ²⁻ + H ₃ O ⁺	1.02 × 10 ⁻²	1.02 × 10 ⁹	-2700	1 × 10 ^{11b,c}

^a Beilke and Gravenhorst (1978); ^b Redlich (1946); ^c Graedel and Weschler (1981).

Table 3. Sulfur chemistry scheme.

Gaseous reaction	k	units
SO ₂ + OH + M → HOSO ₂ + M	4.62 × 10 ⁻³¹ × (T/298.0) ^{-3.90}	cm ⁶ molecule ⁻² s ^{-1a}
HOSO ₂ + O ₂ → HO ₂ + SO ₃	1.30 × 10 ⁻¹² × (-330/T) ^{-3.90}	cm ³ molecule ⁻¹ s ^{-1a}
SO ₃ + H ₂ O → H ₂ SO ₄	9.10 × 10 ⁻¹³	cm ³ molecule ⁻¹ s ^{-1a}
Aqueous reaction	$k(\text{aq.})$	units; (T)
SO _{2(aq.)} + O ₃ → S(VI) + O ₂	2.4 × 10 ⁴	Ms ^{-1b}
HSO ₃ ⁻ + O ₃ → S(VI) + O ₂	3.7 × 10 ⁵	Ms ^{-1b}
SO ₃ ²⁻ + O ₃ → S(VI) + O ₂	1.5 × 10 ⁹	Ms ^{-1b}
HSO ₃ ⁻ + H ₂ O ₂ → S(VI) + H ₂ O	$\frac{k_{\text{H}_2\text{O}_2} \times [\text{H}^+]}{1 + K_{(\text{eq.})} \times [\text{H}^+]}$	Ms ^{-1b}
	with $K_{(\text{eq.})} = 13$	M ^{-1b}
	and $k_{\text{H}_2\text{O}_2} = 7.5 \times 10^7$	M ⁻² s ^{-1b}
S(IV) + $\frac{1}{2}$ O ₂ $\xrightarrow{\text{TMI}}$ S(VI)	750 × [Mn(II)] + 2600 × [Fe(III)] + 1.0 × 10 ¹⁰ [Mn(II)]/[Fe(III)]	s ^{-1c}

^a Atkinson et al. (2004); ^b Hoffmann (1986); ^c Martin and Good (1991).

ual continuity equations of S(IV) species:

$$\begin{aligned} \frac{d[\text{S(IV)}]}{dt} = & -k_{\text{OH}+\text{SO}_2} \times [\text{SO}_2][\text{OH}] \\ & - \sum_j (k_j \times [\text{S(IV)}]_{\text{aq.}} [\text{C}_j]_{\text{aq.}}) - k_d \times [\text{SO}_{2(\text{aq.})} \\ & + \text{HSO}_3^- + \text{SO}_3^{2-}] - K_{\text{mix}} \times ([\text{SO}_2] - [\text{SO}_2]_{(\text{bck.})}), \end{aligned} \quad (8)$$

where k_j the rate constant of the aqueous reaction between oxidant C_j and relevant [S(IV)] species (see the list of aqueous oxidation reaction in Table 3), and k_d is the deposition coefficient of dissolved sulfur species. Dry deposition as such is not expected to be important in the plume itself compared to wet deposition for our cloudy conditions. Since only wet deposition is considered, only species dissolved in water phases such as aqueous S(IV) (SO_{2(aq.)} + HSO₃⁻ + SO₃²⁻) and S(VI) (HSO₄⁻ + SO₄²⁻) species are deposited in the model. The deposition is treated as a first order loss with $k_d = 2 \times 10^{-6} \text{ s}^{-1}$, equivalent to a characteristic time scale of 5.7 days (Stevenson et al., 2003b).

The same approach can be used for S(VI) and deposited S(VI):

$$\begin{aligned} \frac{d[\text{S(VI)}]}{dt} = & k_{\text{OH}+\text{SO}_2} \times [\text{SO}_2][\text{OH}] \\ & + \sum_j (k_j \times [\text{S(IV)}]_{\text{aq.}} [\text{C}_j]_{\text{aq.}}) \\ & - k_d \times [\text{HSO}_4^- + \text{SO}_4^{2-}] \\ & - K_{\text{mix}} \times ([\text{S(VI)}] - [\text{S(VI)}]_{(\text{bck.})}), \end{aligned} \quad (9)$$

$$\frac{d[\text{S(VI)}]_{\text{dep.}}}{dt} = k_d \times [\text{HSO}_4^- + \text{SO}_4^{2-}], \quad (10)$$

where S(VI)_{dep.} is the sulfate deposited at the surface.

2.4 Oxygen isotope signatures in sulfur oxidation

The mass-balance equation describing the production of S(VI) species is coupled to an oxygen isotope transfer scheme in order to track the evolution of $\Delta^{17}\text{O}$ in sulfates in water droplets and in sulfates deposited at the surface. Therefore, the specific isotopic anomaly acquired by a S(VI) molecule (produced by the oxidation of a S(IV) molecule by a specific oxidant) is first derived using isotopic transfer

Table 4. O-MIF signatures of S(IV) oxidation pathways in the model.

Oxidant	O-MIF pathway (‰)
OH	calculated (0 to a maximum of 4.5)
H ₂ O ₂	0.87
O ₃	9
O ₂ /TMI	−0.09

equations. New S(VI) isotopes tracers are then created in order to monitor the amount of isotopic anomaly carried out by sulfates in water droplets and deposited at the surface. They are defined as anomaly products ($\Delta^{17}\text{O} \times [\text{S(VI)}]$), and introduced in the model on the basis of the following continuity equation (Morin et al., 2008, 2011):

$$\begin{aligned} \frac{d}{dt}[\text{S(VI)}] \times \Delta^{17}\text{O}(\text{S(VI)}) & \quad (11) \\ &= \sum_j [P_j \times \Delta^{17}\text{O}(\text{S(VI)}_{\text{prod.}})_j] \\ & - k_d \times \Delta^{17}\text{O}(\text{S(VI)}), \end{aligned}$$

where $\Delta^{17}\text{O}(\text{S(VI)})$ is the isotopic anomaly of atmospheric sulfate, $\Delta^{17}\text{O}(\text{S(VI)}_{\text{prod.}})_j$ is the O-MIF anomaly transferred to sulfate through the specific oxidation channel j , and P_j is the oxidation rate of channel j . $\Delta^{17}\text{O}(\text{S(VI)}_{\text{prod.}})_j$ is fixed for ozone, H₂O₂ and TMI oxidation pathways but it is a prognostic variable for OH (see Table 4).

As deposited sulfate is a variable in the model ($\text{S(VI)}_{\text{dep.}}$), the transfer of isotopic anomaly during deposition is also monitored following a similar equation,

$$\begin{aligned} \frac{d}{dt}[\text{S(VI)}_{\text{dep.}}] \times \Delta^{17}\text{O}(\text{S(VI)}) &= k_d \times [\text{S(VI)}] \\ & \times \Delta^{17}\text{O}(\text{S(VI)}), \end{aligned} \quad (12)$$

The value of oxygen isotopic anomaly (O-MIF) in sulfate depends on the relative importance of individual SO₂ oxidation pathways (P_j) and their respective transfer of O-MIF ($\Delta^{17}\text{O}(\text{S(VI)}_j)$). Note that the continuity equations of S(VI) and $\text{S(VI)}_{\text{dep.}}$ isotopes tracers are integrated with a 4th order Runge–Kutta method algorithm instead of using the CiTTY-CAT chemistry solver with the oxidation rates (i.e. P_j in 11) kept constant over a time step (Morin et al., 2007, 2008). This approach allows keeping the chemistry module totally independent from the oxygen isotopic module. The external integration tool does not affect significantly the results. Throughout this study, it is assumed that both SO₂ and water vapour (H₂O) are not carrying any initial O-MIF. The isotopic composition of magmatic SO₂, indeed follows mass-dependent fractionations and no significant $\Delta^{17}\text{O}$, $\Delta^{34}\text{S}$ and $\Delta^{36}\text{S}$ have been measured so far (Eiler, 2001). Measurements show that tropospheric H₂O does not carry any O-MIF (Uemura et al., 2010), and the same is found for atmospheric SO₂ (Holt

et al., 1981). It is therefore assumed that the O-MIF found in sulfates only originates from the transmission of isotopic anomaly during the aforementioned reactions of sulfur oxidation.

In order to constrain individual SO₂ oxidation pathways from isotopic information, it is first necessary to characterize the specific O-MIFs they transfer to sulfate using isotopic transfer equations.

2.4.1 Oxidation by ozone

The few isotopic measurements of tropospheric ozone indicate values of $\Delta^{17}\text{O}$ (O₃_{bulk}), ranging from 20‰ to 40‰ with a mean value of about 25‰ (Krankowsky et al., 1995; Johnston and Thiemens, 1997; Thiemens, 2006; Vicars and Savarino, 2014). The location of oxygen isotopes within the structure of ozone is not uniform and heavier isotopes are mostly located at the extremities of the molecule (Janssen, 2005; Bhattacharya et al., 2008). Indeed, molecules that have asymmetrical geometrical structures, and bearing heavier oxygen isotopes on terminal sites, are more energetically stable than their symmetric counterparts (Marcus, 2013). This enrichment in heavy oxygen isotopes at terminal locations of ozone is confirmed by laboratory measurements (Bhattacharya et al., 2008). Ozone does not always react with other molecules via terminal oxygen atoms, although this reaction mechanism is energetically favourable since it requires the breaking of only one molecular bond. During the oxidation of reactive nitrogen leading to production of atmospheric nitrate, most of the oxygen atoms involved in the reaction are from terminal sites (Savarino et al., 2008). Multiple studies found a similar selective reactivity indeed, as during photochemical reactions or for reactions of ozone on solid substrates (Sheppard and Walker, 1983; Bhattacharya et al., 2008). Considering the mean bulk O-MIF and terminal isotopic enrichments, a mean reactive ozone O-MIF ($\Delta^{17}\text{O}$ (O₃^{*})) of 36‰ has been derived (Bhattacharya et al., 2008; Savarino et al., 2008; Morin et al., 2007). This value is used throughout this study, since it is in accordance with parametrizations used in previous successful model simulations (Michalski et al., 2003; Alexander et al., 2002; Morin et al., 2007; Alexander et al., 2009; Morin et al., 2011).

The value of O-MIF in sulfates generated during the aqueous oxidation by ozone is determined by identifying the origins of each oxygen atom in sulfate during the reaction of oxidation. Ozone transfers to sulfate only one oxygen atom during aqueous sulfur oxidation, while another oxygen atom derives from the water molecule forming aqueous S(IV). The equation describing the transfer of O-MIF to sulfate during oxidation by ozone is as follows:

$$\begin{aligned} \Delta^{17}\text{O}(\text{S(VI)})_{\text{O}_3+\text{SO}_2} &= \frac{1}{2} \times \Delta^{17}\text{O}(\text{SO}_2) + \frac{1}{4} \\ & \times \Delta^{17}\text{O}(\text{H}_2\text{O}) + \frac{1}{4} \times \Delta^{17}\text{O}(\text{O}_3^*). \end{aligned} \quad (13)$$

This equation can be simplified because the O-MIF anomalies in SO₂ and H₂O are negligible:

$$\Delta^{17}\text{O}(\text{S(VI)})_{\text{O}_3+\text{SO}_2} = \frac{1}{4} \times \Delta^{17}\text{O}(\text{O}_3^*). \quad (14)$$

Therefore, the isotopic anomaly in atmospheric sulfates produced in the model during the oxidation of dissolved SO₂ through O₃ is $\Delta^{17}\text{O}(\text{S(VI)})_{\text{O}_3+\text{SO}_2} = 9\%$ (Morin et al., 2007, 2011).

2.4.2 Oxidation by hydroxyl radical

In the atmosphere, OH radicals are formed as a result of ozone photolysis in presence of water vapour. In particular, ozone photodissociation can produce an O¹(D) radical, which react with a water molecule to produce two OH radicals. Tropospheric OH radicals are thought not to carry O-MIF anomaly because the exchange of oxygen atoms with water vapour is so fast that it erases any inherited isotopic anomaly in OH. Recall that tropospheric H₂O does not carry any O-MIF because the tropospheric H₂O cycle is entirely controlled by physical processes (condensation, evaporation) and not by chemical processes involving ozone. As a result, the O-MIF signature in OH radicals is expected to be 0 ($\Delta^{17}\text{O}(\text{OH}) = 0.0\%$ Morin et al., 2011). However, when the humidity and hence H₂O levels are very low (e.g. upper troposphere), the rate of isotopic exchange between OH radicals and H₂O molecules decreases so much that freshly produced OH radicals may have time to react with other molecules before losing their isotopic anomaly by isotopic exchange with H₂O (Morin et al., 2007). Under those conditions, when the OH loss reactions and cycling compete with the isotopic exchange with H₂O, some of the initial O-MIF originating from ozone is still present in reacting OH. It is also possible for OH loss to compete with the H₂O isotopic exchange when the rate of OH loss is highly enhanced instead of having a reduced rate of H₂O isotopic exchange. This may be the case in volcanic plumes, when SO₂ levels are so high that the SO₂ + OH reaction become the dominant chemical loss (Bekki, 1995), accelerating the OH cycling. In order to account for this possibility, instead of assuming a null O-MIF for OH, the O-MIF in the steady-state OH ($\Delta^{17}\text{O}(\text{OH})$) is calculated explicitly using the approach developed by Morin et al. (Morin et al., 2007). $\Delta^{17}\text{O}(\text{OH})$ is simply derived from the competing balance between the O-MIF erasing isotopic exchange and the total OH loss, typically the reactions with CO and CH₄ in the troposphere. Since we consider sulfur-rich volcanic plumes and clouds, the reaction between OH and SO₂ is also taken into account.

Considering all the transfers of oxygen atoms, the isotopic mass-balance equation for the OH pathway can be expressed as follows:

$$\begin{aligned} \Delta^{17}\text{O}(\text{S(VI)})_{\text{OH}+\text{SO}_2} &= \frac{1}{2} \Delta^{17}\text{O}(\text{SO}_2) \\ &\times + \frac{1}{4} \times \Delta^{17}\text{O}(\text{OH}) + \frac{1}{4} \times \Delta^{17}\text{O}(\text{H}_2\text{O}). \end{aligned} \quad (15)$$

Since tropospheric H₂O and volcanic SO₂ are not thought to carry any O-MIF, the equation can be simplified:

$$\Delta^{17}\text{O}(\text{S(VI)})_{\text{OH}+\text{SO}_2} = \frac{1}{4} \times \Delta^{17}\text{O}(\text{OH}). \quad (16)$$

The O-MIF of OH can be derived using the following equation

$$\Delta^{17}\text{O}(\text{OH}) = x \times \Delta^{17}\text{O}(\text{OH}_{\text{prod.}}^*), \quad (17)$$

with

$$\Delta^{17}\text{O}(\text{OH}_{\text{prod.}}^*) = \frac{1}{2} \times \Delta^{17}\text{O}(\text{O}_3^*), \quad (18)$$

and

$$x = \frac{D}{D + k_{\text{OH}+\text{H}_2\text{O}}^* \times [\text{H}_2\text{O}]} \quad (19)$$

$$\begin{aligned} D &= k_{\text{OH}+\text{CO}} \times [\text{CO}] + k_{\text{OH}+\text{CH}_4} \times [\text{CH}_4] \\ &+ k_{\text{OH}+\text{SO}_2} \times [\text{SO}_2], \end{aligned} \quad (20)$$

where $k_{\text{OH}+\text{H}_2\text{O}}^*$ is the rate constant for the oxygen atoms exchange reaction between OH and H₂O, and $k_{\text{OH}+\text{CH}_4}$ and $k_{\text{OH}+\text{CO}}$ are the reaction rate constants for the gas phase reaction of OH with CH₄ and CO, respectively.

In this approach x represents the competition between the O-MIF erasing effect of isotopic exchange and the O-MIF retaining effect of OH chemical loss; only important loss reactions for tropospheric OH are considered here. $\Delta^{17}\text{O}(\text{OH}_{\text{prod.}}^*)$ is the O-MIF of the OH radical freshly produced, and it is assumed that OH is mostly formed by the photolysis of ozone followed by the reaction of O¹(D) with H₂O.

The O-MIF in OH ($\Delta^{17}\text{O}(\text{OH})$) is determined by this x factor. If OH chemical loss is much faster than the isotopic exchange, $\Delta^{17}\text{O}(\text{OH}) = 0.5 \times \Delta^{17}\text{O}(\text{O}_3^*)$ (i.e. $x = 1$). If chemical loss is much slower than the isotopic exchange, $\Delta^{17}\text{O}(\text{OH}) \approx 0\%$ (i.e. $x \ll 1$).

2.4.3 Oxidation by hydrogen peroxide

In the troposphere, H₂O₂ can quickly dissolve into liquid water phases (Chandler et al., 1988). In a volcanic plume, these phases can be either water droplets or water condensed on solid particles, typically on ash particles. Once in the aqueous phase, H₂O₂ oxidizes SO₂ by nucleophilic displacement, and its two oxygen atoms are transmitted to the produced sulfate molecule (McArdle and Hoffmann, 1983; Brandt and van Eldik, 1995).

The isotopic balance for the oxidation by H₂O₂ in the liquid phase is as follows:

$$\Delta^{17}\text{O}(\text{S(VI)})_{\text{H}_2\text{O}_2+\text{SO}_2} = \frac{1}{2} \times \Delta^{17}\text{O}(\text{SO}_2) + \frac{1}{2} \times \Delta^{17}\text{O}(\text{H}_2\text{O}_2). \quad (21)$$

Since volcanic SO₂ is thought to carry no significant O-MIF, the final O-MIF transfer can be simplified:

$$\Delta^{17}\text{O}(\text{S(VI)})_{\text{H}_2\text{O}_2+\text{SO}_2} = \frac{1}{2} \times \Delta^{17}\text{O}(\text{H}_2\text{O}_2). \quad (22)$$

Isotopic measurements of $\Delta^{17}\text{O}$ of tropospheric H₂O₂ range between 1.30‰ and 2.20‰ with a mean O-MIF of 1.70‰ (Savarino and Thiemens, 1999a, b). Using this mean value, sulfate produced by the H₂O₂ oxidation is assumed to carry a $\Delta^{17}\text{O}(\text{S(VI)})_{\text{H}_2\text{O}_2+\text{SO}_2} = 0.87\%$ (Savarino et al., 2000).

2.4.4 Oxidation by O₂/TMI

Isotopic measurements of atmospheric O₂ indicate that its O-MIF anomaly is rather small (Luz et al., 1999; Barkan and Luz, 2003). Kinetic isotope fractionation associated to the Dole effect (Dole, 1936) and stratospheric influx of O₂ generates a slightly negative O-MIF in tropospheric O₂. As theoretical investigations suggest, a slight depletion of ¹⁷O is indeed found in tropospheric O₂, which is accompanied by a slightly negative O-MIF (Barkan and Luz, 2003). Theoretical calculations predict $\Delta^{17}\text{O}(\text{O}_2)$ as low as -0.344% (Pack et al., 2007) or even, more recently, -0.410% for tropospheric O₂ (Young et al., 2014). Other theoretical calculations suggest a $\Delta^{17}\text{O}(\text{O}_2)$ between 0.141‰ and -0.305% (Young et al., 2002).

We assume a $\Delta^{17}\text{O}(\text{O}_2)$ of -0.340% (Miller, 2002). This value is chosen because it gives a reasonably good agreement between isotopic measurements (Martin et al., 2014) and models (Miller, 2002; Young et al., 2002; Pack et al., 2007). In addition, it has to be kept in mind that there are large uncertainties associated with the exact reaction mechanism of SO₂ oxidation catalysed by TMI. We assume that only one oxygen atom of O₂ is transmitted to sulfate during the SO₂ oxidation (Brandt and van Eldik, 1995; Herrmann et al., 2000).

With these assumptions, the isotopic mass-balance equation for SO₂ oxidation by O₂/TMI is given by

$$\Delta^{17}\text{O}(\text{S(VI)})_{\text{O}_2+\text{SO}_2} = \frac{3}{4} \times \Delta^{17}\text{O}(\text{S(IV)}) + \frac{1}{4} \times \Delta^{17}\text{O}(\text{O}_2). \quad (23)$$

Since volcanic SO₂ is thought to carry no significant O-MIF, we can assume that initial S(IV) species do not carry any O-MIF. Consequently, the isotopic signature associated to this oxidation pathway can be simplified:

$$\Delta^{17}\text{O}(\text{S(VI)})_{\text{O}_2+\text{SO}_2} = \frac{1}{4} \times \Delta^{17}\text{O}(\text{O}_2). \quad (24)$$

$\Delta^{17}\text{O}(\text{O}_2)$ being taken as -0.34% (see above), sulfate produced through this pathway carries a O-MIF ($\Delta^{17}\text{O}(\text{S(VI)})_{\text{O}_2+\text{SO}_2}$) almost null, of about -0.09% (Savarino et al., 2000). The O-MIF signatures of all the S(IV) oxidation pathways used in the model are summarized in Table 4.

3 Box model set-up

3.1 Standard case: initial conditions

All simulations are run for springtime conditions and start at 08:00 at tropical latitudes (8.3° N). In order to reach stable chemical compositions, notably for medium- and short-lived reactive species, the model is run for 3 days before injecting SO₂, then, the evolution of the chemical composition is followed for 7 days. This timescale corresponds approximately to the lifetime of a plume in the free troposphere, in occurrence of low turbulence and low wind shear (Arnold et al., 2007).

Since most of volcanoes are situated in remote areas with their peaks close to the free troposphere, or, at least, with volcanic plumes often ending up in the free troposphere, the environmental conditions are chosen to be representative of the lower free troposphere with temperature set at 283.15 K, and pressure fixed at 640 mbar (about 3 km altitude). Since we consider cloudy conditions, the relative humidity is set to 100 %.

Furthermore, concentrations of reactive species are also set to typical levels found in the tropical lower free troposphere: O₃ = 45 ppbv and H₂O₂ = 0.1 ppbv. Finally, initial SO₂ is set to a mean volcanic plume concentration of 1 ppmv, a value typical of volcanic plumes during degassing (Robock, 2000; Herrmann et al., 2000; Wardell et al., 2004; Mather et al., 2006; Roberts et al., 2012; De Moor et al., 2013; Voigt et al., 2014). The initial pH of the aqueous phase is set to 4.5. It has no impact on the overall model results because the pH is almost immediately driven by SO₂ uptake and sulfur oxidation. Preliminary simulations have shown that the initial SO₂ concentration is a critical input.

Due to the large amounts of water that can be injected during explosive eruptions, in our simulations it is assumed that volcanic water vapour is largely in excess compared to relative humidity of the free troposphere. Moreover, due to low temperature and pressure of the lower free troposphere, for our simulations it is assumed that volcanic water vapour would mostly condense to produce cloud droplets or to coat ash particles. Therefore, throughout this study relative humidity (RH) inside volcanic plumes is set at 100 %, the water saturation point corresponding to the pressure and temperature of the background atmosphere. The Liquid Water Content (LWC) parameterizes the amount of liquid water within plumes. High levels of LWC can be reached, indeed, within volcanic plumes from explosive eruptions. Modelling sim-

ulations suggest that LWC as high as 1.6 g m⁻³ could be reached at the core of water-rich volcanic clouds condensing in the troposphere (Aiuppa et al., 2007). It is possible that, during the first stages of medium-size eruptions, LWC within the plume could be at least comparable to LWC values of growing cumulus clouds. For all the simulations LWC is set to 1.0 g m⁻³, a value between experimental measurements (e.g. meteorological clouds) and modelling studies of water-rich volcanic plumes reaching the upper troposphere (Tabazadeh and Turco, 1993; Hoshyaripour et al., 2015). Like SO₂, LWC is found to be a critical model input.

TMI concentrations in the liquid phase are set to [Fe(III)] = 0.5 μM and to [Mn(II)] = 0.05 μM. These values are at the lower end of typical tropospheric measurements with [Fe(III)] concentrations ranging between 0.5 and 2 μM (Martin, 1984; Martin and Good, 1991; Parazols et al., 2006). Because of uncertainties associated with iron dissolution in volcanic plumes, our TMI concentrations are lower than concentrations found in dust-rich polluted conditions where [Fe(III)] can reach concentrations of around 5 μM (Herrmann et al., 2000; Parazols et al., 2006). TMI concentrations follow the same relation throughout the whole study and for each simulation [Mn(II)] = 0.1 × [Fe(III)] (Martin and Good, 1991).

3.2 Model experiments

The objective of the first set of numerical experiments is to assess the competition among oxidation pathways in SO₂-rich plumes/clouds for the standard case. Three simulations (S1–S3) are run with oxidation schemes of increasing complexity. They simulate oxidation of SO₂: (S1) by OH in gas phase, (S2) by OH in gas phase, and H₂O₂ and O₃ in aqueous phase, and (S3) by OH in gas phase, and H₂O₂, O₃ and O₂/TMI in aqueous phase.

Since initial SO₂ levels, LWC and TMI concentrations in volcanic plumes are relatively uncertain and are key model inputs, the sensitivity of the results to varying conditions within plausible ranges is also explored in additional simulations. Isotopic anomaly transfers are investigated for atmospheric concentrations stretching from passive degassing and quiescent conditions to sulfur-rich volcanic clouds with varying levels of TMI. The intervals used for the different sensitivity studies are summarized in Table 5.

The first set of sensitivity simulations is devoted to the sensitivity of results to initial SO₂ levels in the case of the S1 simulation. It is designed to explore not only the impact of varying SO₂ levels on sulfate O-MIF produced by the OH oxidation pathway, but also on OH isotopic signature itself. Recall that the OH isotopic signature (Δ¹⁷O (OH)) is generally assumed to be 0 in the literature (see Sect. 2.4.2).

It is widely recognized that SO₂ is the compound emitted by volcanic activity which causes the largest climatic impacts through its conversion into sulfate aerosols (Graf et al., 1998; Robock, 2000; Textor et al., 2004; Langmann, 2014). Emis-

Table 5. Ranges of SO₂, LWC and TMI explored in the sensitivity studies.

SO ₂	0.1–10.0 ppmv
LWC	0.1–2.5 g m ⁻³
TMI	0.1–3.0 μM

sions of volcanic SO₂ have been measured both in proximity of volcanic vents and in aged plumes. It is possible to constrain a range of concentrations, considering age of plumes and distance from points of emissions. During the first stages of plume development concentrations of SO₂ in the range of 10–50 ppmv can be reached right in proximity of volcanic vents (Aiuppa et al., 2005, 2006a; Roberts et al., 2012), while concentrations in the range of 0.1–1 ppmv can be found in aged plumes at longer distances from points of emissions (Delmelle, 2003; Carn et al., 2011). These results are confirmed by modelling simulations which can constrain volcanic emissions by accounting for quick dilution after plume ejection from the vent (Gerlach, 2004; Aiuppa et al., 2007; Roberts et al., 2009). Consequently, based on atmospheric simulations and on in situ measurements, the SO₂ concentration is set to 1.0 ppmv in the standard case, and is varied from 0.1 to 10 ppmv in the sensitivity simulations.

LWC plays a crucial role in aqueous oxidation of volcanic SO₂. The range of LWC considered has been chosen based on LWC observed for different cloud typologies such as mean saturated clouds (0.1 g m⁻³), water-rich cumulus clouds (0.5–1 g m⁻³), and cumulonimbus clouds (1–2 g m⁻³) (Laj et al., 1997; Rosenfeld and Lensky, 1998; Pruppacher et al., 1998; Korolev et al., 2007; Carey et al., 2008). LWC is set to 1 g m⁻³ in the standard case and is varied from 0.1 to more extreme values of 2.5 g m⁻³ for sensitivity simulations (Tabazadeh and Turco, 1993; Aiuppa et al., 2007).

Aqueous concentrations of iron ([Fe(tot)] = [Fe(II)] + [Fe(III)]) can peak to 9–10 μM in the troposphere (Desboeufs et al., 1999, 2001) with [Fe(III)] concentrations between 2.0 and 5.0 μM in polluted conditions if photochemical cycling between [Fe(II)]–[Fe(III)] is inhibited (Parazols et al., 2006). Volcanic eruptions inject large quantities of solid material into the atmosphere in the form of ash. As a result, volcanic plumes/clouds are characterized by high concentrations of ash and minerals (Mather et al., 2003). Ash particles have sizes as large as few mm and they are mainly composed of silica and crystalline minerals of magmatic origin. Glass, olivine, magnetite, hematite and fayalite are among the most common minerals injected during eruptions (Rose and Durant, 2009; Langmann, 2014; Hoshyaripour et al., 2015). These minerals are composed in different proportions by Fe(II) and Fe(III), which are entrapped in the crystalline structure of rocks in different morphologies and compositions. Since large quantities of water are also injected during eruptions, water can condense on mineral particles, especially as the volcanic

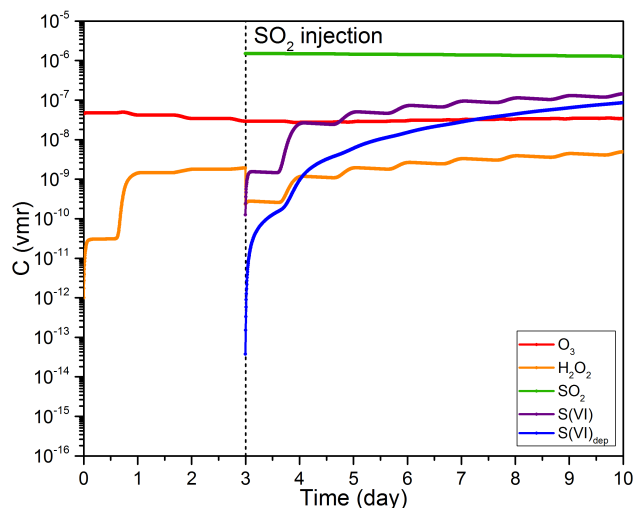


Figure 2. Evolution of the gas-phase concentrations of atmospheric species during the S1 simulation (see text). The simulation starts at 08:00 and SO₂ is injected after 3 days. During the S1 simulation the concentration of injected SO₂ drops from 1.5 ppmv to a final value of 1.27 ppmv.

column reaches higher altitudes and lower temperatures in the troposphere (Tabazadeh and Turco, 1993; Hoshyaripour et al., 2015). Once mineral particles are coated by water, dissolution of iron from the solid mineral surface to the thin liquid water film may take place depending on the acidity of the aqueous phase (Ayrís and Delmelle, 2012; Langmann, 2014; Maters et al., 2016). Acidic conditions (pH < 2.0) due to H₂SO₄ condensation or formation within the liquid phase favour the solubility of minerals containing iron and dissolution of [Fe(III)] (Solmon et al., 2009; Ayrís and Delmelle, 2012). Up to a third of total Fe at the ash surface can dissolve into the liquid phase coating volcanic particles (Hoshyaripour et al., 2014) depending on rock composition and gases in the volcanic clouds. Laboratory experiments on dissolution in acidic water of iron from volcanic ashes suggest that [Fe(III)] concentrations of up to 2 μM can be reached quickly in the liquid phase when pH reaches ~2 (Maters et al., 2016). Concentrations as high as [Fe(III)] = 3 μM could be reached if pH reaches 1 (Maters et al., 2016). Mobilization of iron ions from ashes could be enhanced for plumes reaching the upper troposphere and undergoing ice formation (Jeong et al., 2012; Shi et al., 2012). High concentrations of [Fe(III)] might persist in the liquid phase depending on the lifetime of water droplets, notably driven by evaporation and condensation cycles (Desboeufs et al., 2001; Langmann, 2014).

Cloud properties are affected by evaporation and condensation cycles changing the pH, the size and number of droplets, while formation of insoluble salts at the surface of ash particles entrapped in cloud droplets can affect mobilization of ions (Ayrís and Delmelle, 2012; Langmann, 2014).

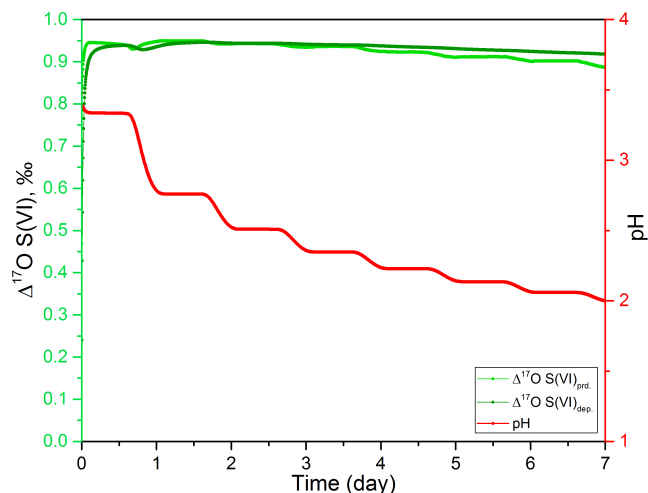


Figure 3. Time evolution of $\Delta^{17}\text{O}(\text{S(VI)})$ in produced and deposited sulfates, and of the pH of the liquid phases in volcanic plumes during simulation S1, following the injection of SO₂ in the box. The change of pH in water droplets is also reported as a function of time.

Therefore, lower acidity combined with the presence of insoluble salts may result in a reduced availability of dissolved TMI in volcanic clouds as the volcanic cloud ages. Over the long term, these conditions can lead to concentration of Fe(III) in water droplets of volcanic clouds which can be lower than typical concentrations found in tropospheric clouds (Desboeufs et al., 1999, 2001). In this study, [Fe(III)] is set to 0.5 g m⁻³ in the standard case and is varied from 0.1 to 3 μM in the sensitivity simulations to cover the wide range of possible [Fe(III)] concentrations.

The resulting model $\Delta^{17}\text{O}(\text{S(VI)})$ (i.e. from standard and sensitivity simulations) are compared to sulfate O-MIF found in tropospheric volcanic sulfates extracted from ash deposits of small and medium-size tropospheric explosive eruptions of the present geological era (Bindeman et al., 2007; Martin et al., 2014; Bao, 2015), or in sulfate aerosols collected at volcanic vents, almost certainly primary sulfate (Mather et al., 2006).

4 Results and discussion

4.1 Isotopic constraints on individual oxidation pathways of volcanic SO₂

4.1.1 Gaseous oxidation by OH

S1 simulates the O-MIF transfer to sulfate in the absence of aqueous oxidation for standard conditions; H₂SO₄ is only produced by the reaction between hydroxyl radicals and SO₂ in the gas phase. As soon as SO₂ is injected, it reacts with OH to produce gaseous H₂SO₄. Figure 2 shows the decay of SO₂ levels from 1.5 to 1.26 ppmv after 7 days.

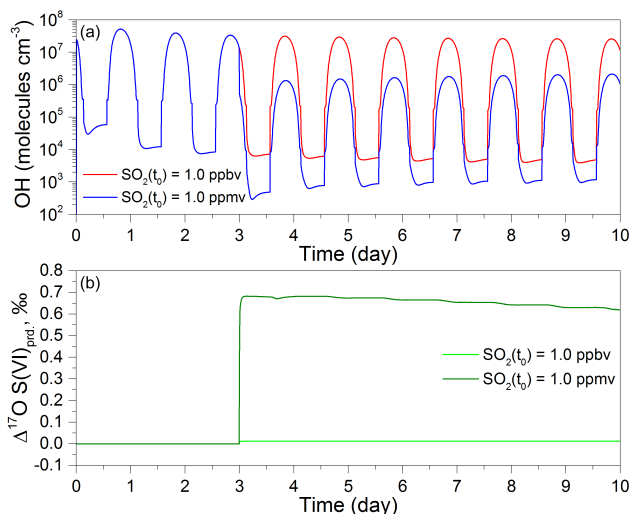


Figure 4. Time evolution of the O-MIF transfer from OH to H₂SO_{4(g)} at two different initial concentrations of SO₂. The light green line represents initial concentration of S(IV) = 1 ppbv (e.g. mean troposphere); the dark green line represents an initial concentration of SO₂ = 1 ppmv (e.g. volcanic plumes and clouds). The upper figure shows concentration trends for OH during the two different scenarios.

As expected, gas-phase concentrations of other SO₂ oxidants (i.e. O₃ and H₂O₂) are not substantially affected by the SO₂ injection. Since H₂SO₄ is very soluble, once produced in the gas phase, it ends up dissolved in the liquid phase where it shifts the pH towards acidic values because of its quasi-complete dissociation. The concentration of atmospheric sulfate (S(VI)) is driven by the gas-phase production and deposition. Sulfate production follows a diurnal cycle because of the diurnal production of OH. There is no significant production of S(VI) during night-time. Figure 3 shows the time evolutions of the liquid phase pH, of the atmospheric sulfate O-MIF ($\Delta^{17}\text{O}(\text{S(VI)})$) and of deposited sulfate O-MIF ($\Delta^{17}\text{O}(\text{S(VI)})_{\text{dep.}}$) following the injection of SO₂. The pH exhibits diurnal variations because sulfate is only produced during daytime. After an initial spike around +0.95‰, atmospheric sulfate O-MIF ($\Delta^{17}\text{O}(\text{S(VI)})$) declines very slowly to +0.9‰ after 7 days. Since SO₂ is only oxidized by OH, the evolution of $\Delta^{17}\text{O}(\text{S(VI)})$ reflects the evolution of the OH isotopic signature ($\Delta^{17}\text{O}(\text{OH})$). Unexpectedly, it is found to be very different from 0. Usually, the exchange of oxygen atoms with water vapour is so fast in the troposphere that it erases any inherited isotopic anomaly in OH. However, in our standard conditions, SO₂ levels are so high that the SO₂ + OH reaction become the overwhelmingly dominant loss (Bekki, 1995) the OH cycling accelerating greatly. Under those conditions, the OH loss is so enhanced that the reaction competes with the isotopic exchange with H₂O. Therefore, OH radicals can react before their isotopic anomaly is entirely erased by the isotopic exchange,

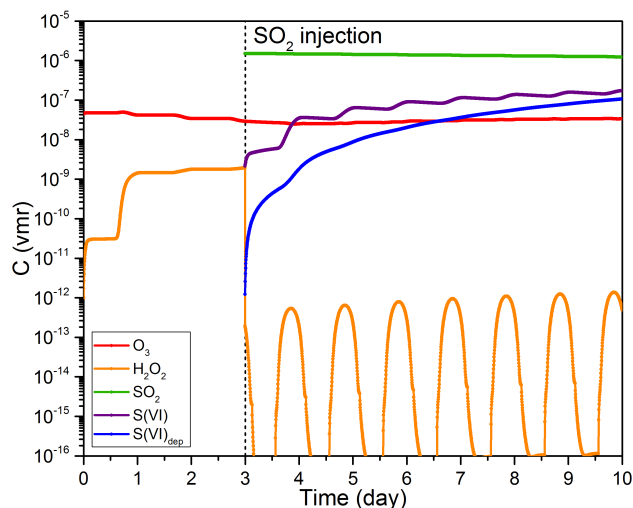


Figure 5. Time evolution in the gas-phase concentrations of SO₂, its tropospheric oxidants and produced and deposited sulfates during S2. During the S2 simulation the concentration of injected SO₂ drops from 1.5 ppmv to a final value of 1.2 ppmv.

and they maintain a significant positive signature. As SO₂ concentration decreases slowly, the rate of OH loss decreases and, as expected, so is $\Delta^{17}\text{O}(\text{S(VI)})$. The evolution of deposited sulfate O-MIF somewhat follows the evolution of the atmospheric sulfate O-MIF but with the time lag which is related to the characteristic timescale of the atmospheric sulfate deposition specified in the model (5.7 days). The final O-MIF of deposited sulfate (resulting from the cumulative effect of sulfate deposited since the SO₂ injection) is 0.92‰, which is distinctively higher than most measurements from volcanic sulfate sampled in volcanic ash deposits (see Table 1).

4.1.2 Isotopic signature of OH: dependence on initial SO₂

Since $\Delta^{17}\text{O}(\text{OH})$ is sensitive to the SO₂ level, additional S1 simulations are carried out with SO₂ concentration differing by 3 orders of magnitude. Figure 4 shows the time evolution of OH and sulfate O-MIF for two different initial SO₂ concentrations (i.e. 1 ppbv and 1 ppmv). The upper plot shows the time evolution of OH for the two SO₂ cases. As soon as the SO₂ is injected, OH concentration drops sharply in the high SO₂ case, whereas it remains unaffected in the low SO₂ case. At such high SO₂ concentrations, the reaction between OH and SO₂ becomes the main OH loss. As a result, OH concentration OH lifetime drop and OH cycling is much faster. The lower plot of Fig. 4 illustrates the effect on the value of O-MIF transferred to sulfate via OH oxidation. For 1 ppbv of initial SO₂ instead of 1 ppmv, $\Delta^{17}\text{O}(\text{OH})$ is negligible (of the order of 0.01‰), thus the sulfate O-MIF is 0. For 1 ppmv of initial SO₂, shortly after the injection, the sulfate produced has an isotopic signature of 0.7‰. It then declines slowly as the SO₂ concentration decays slowly. In

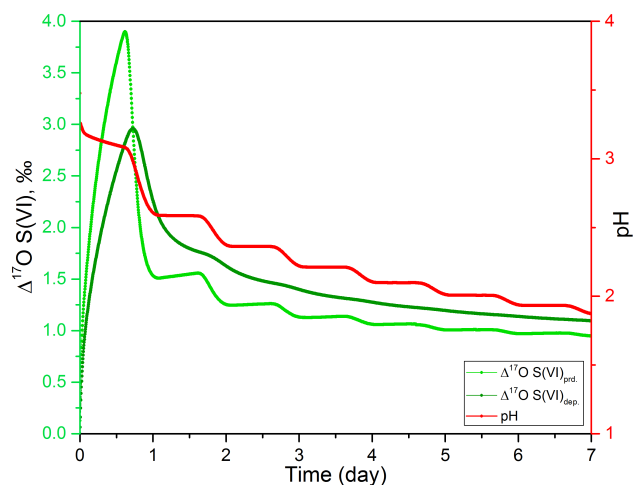


Figure 6. Temporal evolution of $\Delta^{17}\text{O}(\text{S(VI)})$ in produced and deposited sulfates, and of pH during the S2 simulation.

Eq. (17), the competition between OH loss channels and the isotopic exchange with water is represented by the x ratio. In the simulation with 1 ppmv of initial SO₂, $\Delta^{17}\text{O}(\text{OH})$ decreases from 10.8‰ to 7.6‰, whereas the variation is very small in the simulation with 1 ppbv of initial SO₂. These results suggest that OH could have a positive O-MIF in volcanic sulfur-rich plumes and clouds which is subsequently transferred to the produced sulfate. Since most isotopic measurements indicate that O-MIF in volcanic sulfate is very close to zero, at least typically within the measurement errors of about 0.1‰, other oxidation pathways that are mostly mass-dependent (i.e. null O-MIF) have to contribute very significantly to the formation of volcanic sulfate. The other known oxidation pathways of SO₂ are heterogeneous.

4.1.3 Gaseous and heterogeneous oxidation by O₃ and H₂O₂

The S2 simulation is the same as S1 except that it also includes the aqueous oxidation of SO₂ by H₂O₂ and O₃. Figure 5 shows evolving concentrations of atmospheric species as oxidation takes place. Almost as soon as SO₂ is injected, the H₂O₂ concentration drops from about 20 ppbv to less than a pptv. At the same time, as in S1, the pH quickly drops to less than 3 (see Fig. 6). Just after the injection, H₂O₂ is initially the overwhelmingly dominant oxidant (Martin et al., 2014). The contribution of oxidation by O₃ is almost negligible under acidic conditions and the oxidation by OH in the gas phase is initially much slower than aqueous oxidation by H₂O₂. However, as the SO₂ concentration vastly exceeds the H₂O₂ concentration (by 3 orders of magnitude), H₂O₂ is very quickly consumed by reaction with SO₂ in the liquid phase; recall for each molecule of SO₂ oxidized by H₂O₂, one molecule of H₂O₂ is consumed. The difference in concentration between SO₂ and H₂O₂ is such that,

as soon as a molecule of H₂O₂ enters the liquid phase, it is consumed. The sharp drop in H₂O₂ concentration is thus limited by H₂O₂ gas phase diffusion to the surface of the liquid phase, which is followed by its quick reaction with S(IV). After the initial drop, the H₂O₂ concentration stays very low with very large diurnal variations. The daytime concentration approaches pptv levels because the loss to the liquid phase is balanced by gas-phase photochemical production. After the drop in H₂O₂, most of the SO₂ is oxidized by OH in the gas-phase. As shown in Fig. 6, the pH in S2 follows a trend similar to the one in S1. The sulfate O-MIF in S2 is higher than in S1. In the first phase, sulfate is produced with a rather high O-MIF signature because the contribution of O₃ to SO₂ oxidation is significant with an initial pH set to 4.5 (i.e. as high as 50% of SO₂ is oxidized by O₃ within the first hours). The O-MIF of produced sulfate ($\Delta^{17}\text{O}(\text{S(VI)})_{\text{prd.}}$) peaks early on at 4‰. However, the pH drops very quickly as more S(VI) is produced in the aqueous phase. As a result, the pH-dependent oxidation rate by O₃ decreases quickly and hence so does $\Delta^{17}\text{O}(\text{S(VI)})_{\text{prd.}}$. H₂O₂ is completely consumed within 15 min during the first timesteps, and it does not contribute to the SO₂ oxidation thereafter. The oxidation of SO₂ is dominated by OH except during the early phase. The final O-MIF in deposited sulfate is 1.1‰, originating mostly from OH oxidation. Recall that, when OH is generated via its main production channel, it carries an isotopic anomaly. Under common (non-volcanic) conditions, the OH anomaly is so rapidly erased by isotopic exchange with H₂O that, when OH reacts, it carries no anomaly. However, when SO₂ levels are very high, OH might react very quickly with SO₂ without having lost its anomaly by isotopic exchange. In this situation, the value of $\Delta^{17}\text{O}(\text{OH})$ is determined by the competition between the SO₂ + OH reaction and the OH isotopic exchange with H₂O. As SO₂ concentration decays with time, $\Delta^{17}\text{O}(\text{OH})$ decreases because the SO₂ + OH reaction slows down and becomes less competitive with respect to the isotopic exchange (see Eq. 15–20). This explains why $\Delta^{17}\text{O}(\text{OH})$ decreases from 4‰ to roughly 3‰ by the end of the simulation, resulting in produced sulfates with O-MIF of 1 and 0.75‰, respectively. The value of O-MIF on deposited sulfates produced in this simulation is still much higher than most O-MIF measurements in tropospheric volcanic sulfates (see Table 1). In order to produce mass-dependent sulfates without O-MIF ($\Delta^{17}\text{O} = 0.0 \pm 0.1$ ‰), another oxidant needs to be dominant and it has to carry a small or null O-MIF anomaly.

4.1.4 Gaseous and heterogeneous oxidation by O₃, H₂O₂ and O₂/TMI

Simulation S3 includes all the major pathways of oxidation involved during formation of sulfate in SO₂-rich clouds (i.e. without significant halogens concentrations compared to sulfur species). Figure 7 shows the evolution of the chemical species concentrations. In S3, H₂O₂ is very quickly depleted

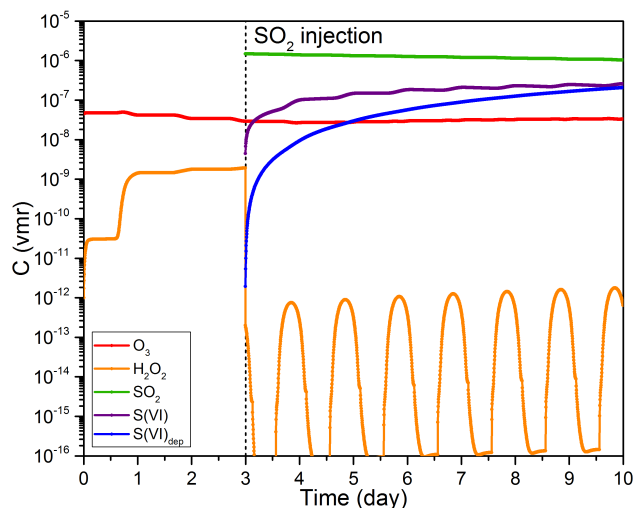


Figure 7. Time evolution in the gas-phase concentrations of SO₂, its tropospheric oxidants and produced and deposited sulfates during S3. During the S3 simulation the concentration of injected SO₂ drops from 1.5 ppmv to a final value of 1 ppmv.

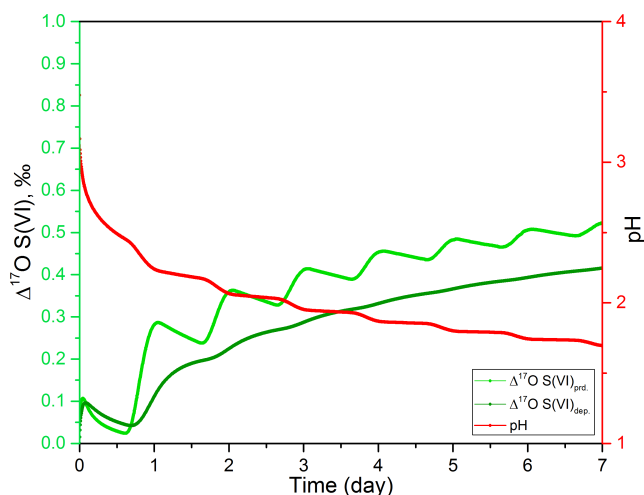


Figure 8. Time evolution of $\Delta^{17}\text{O}(\text{S}(\text{VI}))$ in produced and deposited sulfates, and of pH of the liquid phases of volcanic plumes during simulation S3.

just after the SO₂ injection as in S2. However, there is much less SO₂ left at the end of the run in S3 than in S2 and S1 and conversely there is more S(VI) produced in S3 than in S2 and S1. With the TMI catalysed oxidation added to the S2 chemical scheme, heterogeneous chemistry becomes competitive with the gas-phase oxidation by OH and lead to faster formation of S(VI). The pH is also lower (see Fig. 8), confirming that more sulfates are in aqueous solution. The final O-MIF in deposited sulfates is about 0.3%. This value is lower than the values calculated in simulations S1 and S2 and closer but still higher than the range of isotopic measurements carried out on volcanic sulfate (see Table 1). This result suggests

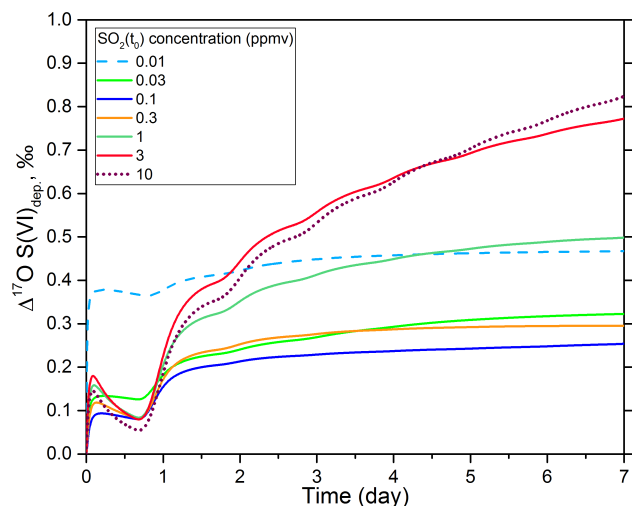


Figure 9. Temporal evolution of $\Delta^{17}\text{O}(\text{S}(\text{VI}))_{\text{dep}}$ at different initial concentrations of SO₂. The dashed line represents simulation where H₂O₂ is the major SO₂ oxidant, straight lines are simulations for which OH is the major oxidant, and dotted lines are simulations for which O₂/TMI is the major pathway of oxidation. The equivalent pathways contributions are summarized in Table 6. Other critical parameters are set as follows: LWC = 1.0 g m⁻³ and [Fe(III)] = 0.5 μM.

that heterogeneous SO₂ oxidation by O₂/TMI is the only pathway able to explain sulfate isotopic measurements with the current chemical scheme. Sensitivity studies are however needed to test the responses of the system to varying conditions of heterogeneous oxidation. Consequently, we conduct further simulations to probe the effects of LWC and TMI aqueous concentrations on the final MIF in deposited sulfate and assess the robustness of the overall results.

4.2 Sensitivity studies

4.2.1 Influence of SO₂ on sulfate O-MIF

In the first set of sensitivity simulations (Z1), the response of the system to various concentrations of SO₂ is tested for the standard conditions with all the oxidation channels included in the model. Figure 9 shows the time evolution of O-MIF in the produced sulfate for different initial SO₂ concentrations. The initial concentration of volcanic SO₂ is varied from 10 ppbv to 10.0 ppmv. LWC is set to 1.0 g m⁻³ and [Fe(III)] = 0.5 μM. The response of the system and, in particular, of produced sulfate O-MIF to varying SO₂ levels is complex and not at all linear. In Table 6 the different contributions of the oxidation pathways are reported for different initial SO₂ concentrations, in the functions of O-MIF in OH and O-MIF in deposited sulfate. The isotopic anomalies and the contribution of different pathways of oxidation are reported for 1 day after sulfur injection, and for the end of the simulations. For an initial SO₂ of 10 ppbv, H₂O₂ is

Table 6. Contribution to sulfate production from different pathways of sulfur oxidation at varying initial concentration of SO₂.

C ₀ , SO ₂ (ppmv)	Time (day)	Δ ¹⁷ O(OH) (‰)	OH	O ₃	H ₂ O ₂	O ₂ /TMI	Δ ¹⁷ O(S(VI), dep.) _f (‰)
0.01	1	0	39	0	55	6	0.38
	7	0	35	0	60	5	0.47
0.03	1	0	60	0	30	10	0.18
	7	0	54	0	40	6	0.32
0.1	1	0.3	63	0	22	15	0.15
	7	0.05	66	0	28	6	0.32
0.3	1	0.8	56	0	19	25	0.17
	7	0.3	69	0	22	9	0.29
1	1	2.6	43	0	15	42	0.20
	7	2	62	0	19	19	0.50
3	1	6.2	30	0	10	60	0.23
	7	5.6	51	0	14	35	0.77
10	1	11.5	17	0	5	77	0.19
	7	11.2	33	0	9	58	0.82

the dominant pathway of sulfur oxidation with the OH oxidation pathway representing about a third of the total; the final O-MIF in the deposited sulfate is 0.50‰. When the initial SO₂ concentration is increased (from 10 ppbv to 30 and then 100 ppbv), sulfate O-MIF decreases because the H₂O₂ contribution to SO₂ oxidation drops whereas the OH contribution becomes dominant. The drop in the H₂O₂ contribution is mostly due to the increased acidity of cloud droplets at higher SO₂ concentrations, resulting in much reduced uptake of SO₂ combined to a much smaller fraction of aqueous S(IV) in the form of HSO₃⁻, the reactant for the S(IV) oxidation by H₂O₂ (McArdle and Hoffmann, 1983). Above 100 ppbv, instead of decreasing, sulfate O-MIF increases at higher initial SO₂ concentration, with 10 ppmv being the maximum SO₂ concentration considered here. This inversion in the evolution of Δ¹⁷O(S(VI)) with increasing SO₂ concentration originates from the change in Δ¹⁷O(OH). Up to 100 ppbv of SO₂, Δ¹⁷O(OH) is more or less negligible and consequently the OH oxidation produces sulfate with insignificant O-MIF. However, at 300 ppbv of initial SO₂, Δ¹⁷O(OH) is equal to 0.8‰ at the start of simulation and is still greater than 0.3‰ at the end of the run. The higher SO₂ concentration is, the higher Δ¹⁷O(OH) is. At 10 ppmv of SO₂, Δ¹⁷O(OH) = 11.5‰. Recall that the maximum possible value of Δ¹⁷O(OH) is 18.0‰, corresponding to conditions where the rate of the isotopic exchange is negligible compared to the rate of OH chemical loss. Interestingly, the overall contribution of OH to the sulfur oxidation peaks at 69% for initial SO₂ equal to 300 ppbv. At higher concentrations, the OH contribution decreases reaching 33% for the simulation with 10 ppmv of initial SO₂. At the same time, the contribution of O₂/TMI oxidation (the

only channel with a negligible O-MIF signature) increases sharply becoming even dominant (58%) for the simulation with 10 ppmv of initial SO₂. Nonetheless, the very large increase in Δ¹⁷O(OH) is the main driver of Δ¹⁷O(S(VI)) for high SO₂ levels, because the OH contribution remains important even for the simulation with 10 ppmv of initial SO₂. Note that the H₂O₂ contribution declines all the way with increasing initial SO₂ (from 10 ppbv to 10 ppmv) which is the inverse of the O₂/TMI contribution evolution.

Overall, the model-calculated contribution of the OH pathway to volcanic sulfur oxidation does not drop below 30% for the standard conditions considered here. As a result, the O-MIF of deposited sulfate O-MIF is expected to depend strongly on the amount of SO₂ injected, via the dependency of OH isotopic signature on SO₂ concentration. Since volcanic SO₂ usually reaches ppmv levels during the first stages of volcanic plume (Roberts et al., 2009, 2012; Oppenheimer et al., 2013; Voigt et al., 2014), our results suggest that volcanic sulfate should carry positive O-MIF anomalies that exceed isotopic measurement uncertainties (≈ 0.1‰). This is not supported by atmospheric measurements of volcanic sulfate isotopic composition which mostly lie close to zero within measurement uncertainties. Other environmental conditions or reaction mechanisms have to be considered to explain the lack of O-MIF in volcanic sulfate

4.2.2 Influence of LWC on sulfate O-MIF

The second set of sensitivity runs (Z2) tests the influence of the LWC amount on model results, notably the final sulfate O-MIF. Fe(III) aqueous concentration is fixed to 0.5 μM, and the initial concentration of SO₂ is set to 1.5 ppmv. Figure 10

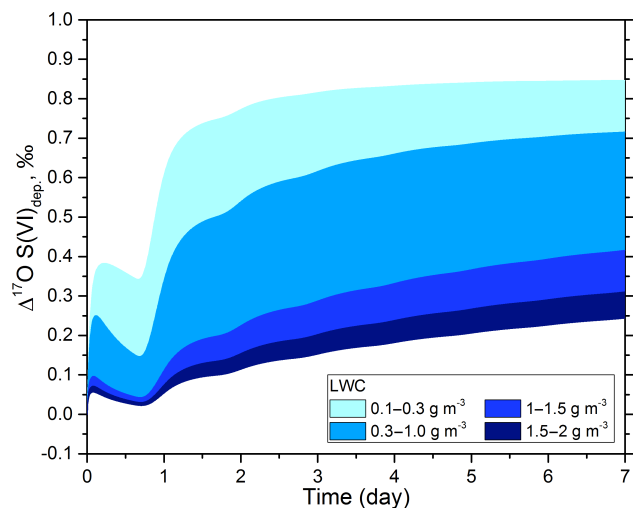


Figure 10. Temporal evolution of $\Delta^{17}\text{O}(\text{S}(\text{VI}))_{\text{dep.}}$ at different values of liquid water content. Other initial critical parameters are set as follows: $[\text{Fe}(\text{III})] = 0.5 \mu\text{M}$ and $[\text{SO}_2]_0 = 1.5 \text{ ppmv}$.

shows the evolution of $\Delta^{17}\text{O}(\text{S}(\text{VI}), \text{dep.})$ for varying LWC. Unlike the influence of SO₂, sulfate O-MIF is a monotonic function of LWC. The higher the LWC is, the lower the sulfate O-MIF is. Higher values of LWC favours higher dissolution rate of SO₂ in droplets and push the dynamics of oxidation towards liquid phase reactions. Also, at high LWC, H₂O₂ is more quickly depleted from the gas-phase because of faster uptake in the liquid phase. Overall, higher LWC favours the O₂/TMI oxidation pathway since lower acid concentration promotes the dissolution of SO₂ in the aqueous phase. Higher LWC does not directly affect the vapour pressure of the system, because it is assumed that cloud droplets are formed at high water saturation. Therefore, changes in cloud LWC do not affect the isotopic composition of produced OH. For the range of LWC considered here (from 0.1 to 3 g m⁻³), the final O-MIF of deposited sulfate varies from 0.8 ‰ to 0.2 ‰. The results show that, in volcanic clouds and plumes, sulfate O-MIF is affected by the LWC value. However, high LWCs alone do not appear to be sufficient to reproduce most of the isotopic measurements in volcanic sulfate.

4.2.3 Influence of TMI on sulfate O-MIF

The third and last set of sensitivity runs (Z3) tests the influence of TMI concentrations on model results, notably the final sulfate O-MIF. Laboratory experiments on iron mobilization from ash indicate that an average concentrations of $[\text{TMI}] = 3 \mu\text{M}$ could be reached within the first hour of ash exposure to very acidic water in the case of silica ashes (Maters et al., 2017). According to the measurements, concentration of dissolved $[\text{Fe}(\text{III})]$ generally varies in the range of 0.1 to 2 μM depending on the mineral composition (Hoshyaripour et al., 2015; Maters et al., 2016, 2017). However, there is a lot of uncertainty on the typical concentrations

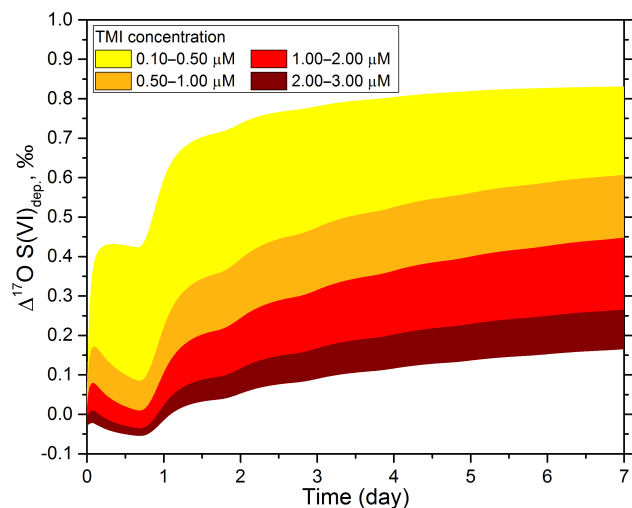


Figure 11. Temporal evolution of $\Delta^{17}\text{O}(\text{S}(\text{VI}))_{\text{dep.}}$ at different concentrations of TMI in aqueous solution. Other initial parameters were set: $\text{LWC} = 1.0 \text{ g m}^{-3}$ and $[\text{SO}_2]_0 = 1.5 \text{ ppmv}$.

of dissolved iron mobilized in volcanic plumes. In Fig. 11, the plot shows the evolution of deposited sulfate O-MIF to varying concentrations of dissolved TMI (from 0.1 to 3 μM). At relatively low concentrations of dissolved Fe(III) (0.1–1.0 μM), deposited sulfates are generated with high O-MIFs and a final O-MIF greater than 0.4 ‰. At higher concentrations of $[\text{Fe}(\text{III})] = 2$ or 3 μM , deposited sulfate O-MIF reaches values as low as 0.25 ‰ and 0.15 ‰, respectively. According to the laboratory experiments, these high Fe(III) concentrations require a pH below $\text{pH} \leq 2$, enhancing the mobilization of $[\text{Fe}(\text{III})]$. In the simulations, the pH is close to this threshold value (see Fig. 8). In conclusion, the model simulations suggest that deposited sulfate with very low O-MIF values, consistent with most isotopic measurements of volcanic secondary sulfate (less than 0.1 ‰), can only be achieved with highly enhanced Fe(III) mobilization.

5 Conclusions

We use the tropospheric photochemical box model CiTTY-CAT to analyse why most oxygen isotopic measurements of tropospheric volcanic sulfate indicate that volcanic sulfates are essentially mass-dependent (i.e. O-MIF anomalies lying close to zero within measurement uncertainties of $\pm 0.1 \text{ ‰}$ typically). This is also observed for volcanic sulfate collected very far from volcanoes where secondary sulfate (produced by oxidation of volcanic sulfur precursors, mostly SO₂) is expected to vastly dominate. This lack of O-MIF in volcanic sulfate is rather intriguing because secondary sulfates originating from other sources exhibit significant O-MIF. A major difference between volcanic sulfur and other sources is that it is often emitted within very dense volcanic plumes whose chemical compositions are radically different from

background air. The chemical environment of the plumes may affect the oxidation pathways and hence sulfate isotopic composition.

A new sulfur isotopic O-MIF scheme is implemented in the model in order to monitor the transfer of O-MIF from oxidants to sulfate during the oxidation of volcanic SO₂. A range of simulations are performed in order to explore in details the different pathways of SO₂ oxidation (gas-phase oxidation by OH and aqueous oxidation by O₃, H₂O₂ and O₂/TMI) and, more importantly for O-MIF, their relative importance for a range of possible volcanic conditions. The first salient finding is that, according to the model calculations, OH should carry a very significant O-MIF in sulfur-rich volcanic plumes. This implies that, when volcanic sulfate is produced in the gas phase via SO₂ oxidation by OH, its O-MIF should have a very significant positive value. Since most isotopic measurements of volcanic sulfate do not indicate the presence of O-MIF, the OH oxidation pathway cannot be the dominant channel for volcanic sulfur. Nonetheless, uncertainties in the rate constant of the isotopic exchange between OH and H₂O (Dubey et al., 1997) and, more generally, on photochemical modelling are substantial (Ridley et al., 2017). It would be useful for this unexpected model predictions of O-MIF in OH, and hence volcanic sulfate produced in gas phase, to be tested in a controlled environment, ideally with laboratory experiments of SO₂ oxidation with a well constrained OH chemical budget, especially in relation to the loss processes. The second important finding from these simulations is that, although H₂O₂ is a major oxidant of SO₂ throughout the troposphere, it is very rapidly consumed in sulfur-rich volcanic plumes. Since H₂O₂ produced within the plume and the entrainment of H₂O₂ from the atmospheric background also represent relatively weak sources, H₂O₂ is found to be a minor oxidant for volcanic SO₂ whatever the liquid water content. According to the simulations, oxidation of SO₂ by O₃ is negligible because volcanic aqueous phases are too acidic. The model predictions of minor or negligible sulfur oxidation by H₂O₂ and O₃, two oxidants carrying large O-MIF, are consistent with the lack of O-MIF seen in isotopic measurements of volcanic tropospheric sulfate. The third finding is that oxidation by O₂/TMI in volcanic plumes could be very substantial and, in some cases, dominant, notably because the rates of SO₂ oxidation by OH, H₂O₂, and O₃ are vastly reduced in a volcanic plume compared to the background air. Only cases where sulfur oxidation by O₂/TMI is very dominant can explain the isotopic measurements of volcanic tropospheric sulfate. We stress that oxidation by O₂/TMI is poorly constrained in model simulations because of the lack of measurements of TMI aqueous concentrations in volcanic plumes. It is worth pointing out that our model results are only applicable to cloudy volcanic plumes. Nonetheless, water clouds do not always form in volcanic plumes, notably during passive degassing. It would be interesting to also consider cloud-free plumes where the condensed phase is concentrated sulfuric

acid within sulfate aerosols. In particular, these particles have a chemical reactivity radically different from water droplets.

A potentially significant limitation of the model simulations is the omission of volcanic halogens. Indeed, volcanic halogens are known to undergo multi-phase chemistry, resulting in ozone depletion and possibly impacting the oxidation of volcanic SO₂ (Bobrowski et al., 2003; Bobrowski and Platt, 2007; Millard et al., 2006; Bobrowski et al., 2007; Roberts et al., 2009; von Glasow, 2010; Roberts et al., 2014; Jourdain et al., 2016). Halogen species such as HOBr may also directly oxidize SO₂ in the aqueous phase (Chen et al., 2017), but this oxidation pathway has not been quantified yet for volcanic plumes. Overall, the present simulations might only be representative of degassing or eruptions with extremely low halogen emissions, typically originating from intraplate and rift volcanic activity. It is certainly worth exploring the potential impact of halogens in the case of halogen-rich eruptions, notably for volcanic plumes where water does not condense and hence only sulfate aerosols are present. Since the heterogeneous conversion of halogen halides into radicals is known to be fast on sulfate aerosols (Bobrowski et al., 2007; Roberts et al., 2009; von Glasow, 2010; von Glasow and Crutzen, 2013), halogens might significantly impact the plume chemistry and the isotopic composition of secondary sulfate for halogens rich conditions.

Data availability. The CiTTyCAT data and model used in this study are archived at LATMOS, and available on request from the lead author (galeazzo.tommaso@latmos.ipsl.fr; tommaso.galeazzo@gmail.com).

Author contributions. TG, SB, EM, and JS designed the study. SA provided the initial version of the model. TG carried out the research, and performed data analysis. TG and SB wrote the manuscript with contributions from all authors. All authors have given approval to the final version of the manuscript.

Competing interests. The authors declare that they have no conflict of interest.

Acknowledgements. We would like to thank the two reviewers for their constructive comments. Discussions with Elena Maters and Gholamali Hoshiyaripour were also useful to address issues related to TMI concentrations in aqueous solution of in-plume water phases. The Agence Nationale de la Recherche (ANR) via contract 14-CE33-0009-02-FOFAMIFS is acknowledged for its financial support.

Edited by: Eliza Harris

Reviewed by: two anonymous referees

References

- Aiuppa, A.: Degassing of halogens from basaltic volcanism: Insights from volcanic gas observations, *Chem. Geol.*, 263, 99–109, <https://doi.org/10.1016/j.chemgeo.2008.08.022>, 2009.
- Aiuppa, A., Inguaggiato, S., McGonigle, A. J., O'Dwyer, M., Oppenheimer, C., Padgett, M. J., Rouwet, D., and Valenza, M.: H₂S fluxes from Mt. Etna, Stromboli, and Vulcano (Italy) and implications for the sulfur budget at volcanoes, *Geochim. Cosmochim. Acta.*, 69, 1861–1871, <https://doi.org/10.1016/j.gca.2004.09.018>, 2005.
- Aiuppa, A., Federico, C., Giudice, G., Gurrieri, S., Liuzzo, M., Shinohara, H., Favarra, R., and Valenza, M.: Rates of carbon dioxide plume degassing from Mount Etna volcano, *J. Geophys. Res.-Sol. Ea.*, 111, 1–8, <https://doi.org/10.1029/2006JB004307>, 2006.
- Aiuppa, A., Franco, A., von Glasow, R., Allen, A. G., D'Alessandro, W., Mather, T. A., Pyle, D. M., and Valenza, M.: The tropospheric processing of acidic gases and hydrogen sulphide in volcanic gas plumes as inferred from field and model investigations, *Atmos. Chem. Phys.*, 7, 1441–1450, <https://doi.org/10.5194/acp-7-1441-2007>, 2007.
- Alexander, B., Savarino, J., Barkov, N. I., Delmas, R. J., and Thiemens, M. H.: Climate driven changes in the oxidation pathways of atmospheric sulfur, *Geophys. Res. Lett.*, 29, 30–1–30–4, <https://doi.org/10.1029/2002GL014879>, 2002.
- Alexander, B., Park, R. J., Jacob, D. J., Li, Q. B., Yantosca, R. M., Savarino, J., Lee, C. C. W., and Thiemens, M. H.: Sulfate formation in sea-salt aerosols: Constraints from oxygen isotopes, *J. Geophys. Res.-Atmos.*, 110, 1–12, <https://doi.org/10.1029/2004JD005659>, 2005.
- Alexander, B., Park, R. J., Jacob, D. J., and Gong, S.: Transition metal-catalyzed oxidation of atmospheric sulfur: Global implications for the sulfur budget, *J. Geophys. Res.-Atmos.*, 114, 1–13, <https://doi.org/10.1029/2008JD010486>, 2009.
- Allen, A. G., Oppenheimer, C., Ferm, M., Baxter, P. J., Horrocks, L. A., Galle, B., McGonigle, A. J. S., and Duffell, H. J.: Primary sulfate aerosol and associated emissions from Masaya Volcano, Nicaragua, *J. Geophys. Res.-Atmos.*, 107, 4682, <https://doi.org/10.1029/2002JD002120>, 2002.
- Andres, R. J. and Kasgnoc, a. D.: A time-averaged inventory of sub-aerial volcanic sulfur emissions, *J. Geophys. Res.*, 103, 25251, <https://doi.org/10.1029/98JD02091>, 1998.
- Arnold, S. R., Methven, J., Evans, M. J., Chipperfield, M. P., Lewis, A. C., Hopkins, J. R., McQuaid, J. B., Watson, N., Purvis, R. M., Lee, J. D., Atlas, E. L., Blake, D. R., and Rappenglück, B.: Statistical inference of OH concentrations and air mass dilution rates from successive observations of nonmethane hydrocarbons in single air masses, *J. Geophys. Res.-Atmos.*, 112, 1–15, <https://doi.org/10.1029/2006JD007594>, 2007.
- Atkinson, R., Baulch, D. L., Cox, R. A., Crowley, J. N., Hampson, R. F., Hynes, R. G., Jenkin, M. E., Rossi, M. J., and Troe, J.: Evaluated kinetic and photochemical data for atmospheric chemistry: Volume I – gas phase reactions of O_x, HO_x, NO_x and SO_x species, *Atmos. Chem. Phys.*, 4, 1461–1738, <https://doi.org/10.5194/acp-4-1461-2004>, 2004.
- Ayris, P. and Delmelle, P.: Volcanic and atmospheric controls on ash iron solubility: A review, *Phys. Chem. Earth*, 45–46, 103–112, <https://doi.org/10.1016/j.pce.2011.04.013>, 2012.
- Bao, H.: Sulfate : A time capsule for Earth' s O₂, O₃, and H₂O, *Chem. Geol.*, 395, 108–118, <https://doi.org/10.1016/j.chemgeo.2014.11.025>, 2015.
- Bao, H., Thiemens, M. H., Farquhar, J., Campbell, D. A., Lee, C. C.-W., Heine, K., and Loope, D. B.: Anomalous ¹⁷O compositions in massive sulphate deposits on the Earth, *Nature*, 406, 176–178, <https://doi.org/10.1038/35018052>, 2000.
- Bao, H., Thiemens, M. H., Loope, D. B., and Yuan, X. L.: Sulfate oxygen-17 anomaly in an Oligocene ash bed in mid-North America: Was it the dry fogs?, *Geophys. Res. Lett.*, 30, 1843, <https://doi.org/10.1029/2003GL016869>, 2003.
- Barkan, E. and Luz, B.: High-precision measurements of ¹⁷O/¹⁶O and ¹⁸O/¹⁶O of O₂ and O₂/Ar ratio in air, *Rapid Commun. Mass Spectrom.*, 17, 2809–2814, <https://doi.org/10.1002/rcm.1267>, 2003.
- Baroni, M., Thiemens, M. H., Delmas, R. J., and Savarino, J.: Mass-Independent Sulfur Isotopic Compositions in Stratospheric Volcanic Eruptions, *Science*, 315, 84–87, <https://doi.org/10.1126/science.1131754>, 2007.
- Bates, T. S., Lamb, B. K., Guenther, A., Dignon, J., and Stoiber, R. E.: Sulfur emissions to the atmosphere from natural sources, *J. Atmos. Chem.*, 14, 315–337, <https://doi.org/10.1007/BF00115242>, 1992.
- Beilke, S. and Gravenhorst, G.: Heterogeneous SO₂-oxidation in the droplet phase, *Atmos. Environ.*, 12, 231–239, [https://doi.org/10.1016/0004-6981\(78\)90203-2](https://doi.org/10.1016/0004-6981(78)90203-2), 1978.
- Bekki, S.: Oxidation of volcanic SO₂: A sink for stratospheric OH and H₂O, *Geophys. Res. Lett.*, 22, 913–916, <https://doi.org/10.1029/95GL00534>, 1995.
- Berglen, T. F., Berntsen, T. K., Isaksen, I. S. A., and Sundet, J. K.: A global model of the coupled sulfur/oxidant chemistry in the troposphere: The sulfur cycle, *J. Geophys. Res.-Atmos.*, 109, D19310, <https://doi.org/10.1029/2003JD003948>, 2004.
- Bhattacharya, S. K., Pandey, A., and Savarino, J.: Determination of intramolecular isotope distribution of ozone by oxidation reaction with silver metal, *J. Geophys. Res.*, 113, D03303, <https://doi.org/10.1029/2006JD008309>, 2008.
- Bindeman, I. N., Eiler, J. M., Wing, B. A., and Farquhar, J.: Rare sulfur and triple oxygen isotope geochemistry of volcanogenic sulfate aerosols, *Geochim. Cosmochim. Acta.*, 71, 2326–2343, <https://doi.org/10.1016/j.gca.2007.01.026>, 2007.
- Bobrowski, N. and Platt, U.: SO₂/BrO ratios studied in five volcanic plumes, *J. Volcanol. Geotherm. Res.*, 166, 147–160, <https://doi.org/10.1016/j.jvolgeores.2007.07.003>, 2007.
- Bobrowski, N., Hönninger, G., Galle, B., and Platt, U.: Detection of bromine monoxide in a volcanic plume, *Nature*, 423, 273–276, <https://doi.org/10.1038/nature01625>, 2003.
- Bobrowski, N., von Glasow, R., Aiuppa, A., Inguaggiato, S., Louban, I., Ibrahim, O. W., and Platt, U.: Reactive halogen chemistry in volcanic plumes, *J. Geophys. Res.-Atmos.*, 112, 1–17, <https://doi.org/10.1029/2006JD007206>, 2007.
- Brandt, C. and van Eldik, R.: Transition Metal-Catalyzed Oxidation of Sulfur(IV) Oxides. Atmospheric-Relevant Processes and Mechanisms, *Chem. Rev.*, 95, 119–190, <https://doi.org/10.1021/cr00033a006>, 1995.
- Brandt, C., Fábíán, I., and van Eldik, R.: Kinetics and Mechanism of the Iron(III)-catalyzed Autoxidation of Sulfur(IV) Oxides in Aqueous Solution. Evidence for the Redox Cycling of Iron in the Presence of Oxygen and Modeling of

- the Overall Reaction Mechanism, *Inorg. Chem.*, 33, 687–701, <https://doi.org/10.1021/ic00082a012>, 1994.
- Brenninkmeijer, C. A. M., Janssen, C., Kaiser, J., Röckmann, T., Rhee, T. S., and Assonov, S. S.: Isotope effects in the chemistry of atmospheric trace compounds., *Chem. Rev.*, 103, 5125–5162, <https://doi.org/10.1021/cr020644k>, 2003.
- Calvert, J. G., Su, F., Bottenheim, J. W., and Strausz, O. P.: Mechanism of the homogeneous oxidation of sulfur dioxide in the troposphere, *Atmos. Environ.*, 12, 197–226, [https://doi.org/10.1016/0004-6981\(78\)90201-9](https://doi.org/10.1016/0004-6981(78)90201-9), 1978.
- Carey, L. D., Niu, J., Yang, P., Kankiewicz, J. A., Larson, V. E., and Vonder Haar, T. H.: The vertical profile of liquid and ice water content in midlatitude mixed-phase altocumulus clouds, *J. Appl. Meteorol. Climatol.*, 47, 2487–2495, <https://doi.org/10.1175/2008JAMC1885.1>, 2008.
- Carn, S. A., Froyd, K. D., Anderson, B. E., Wennberg, P., Crouse, J., Spencer, K., Dibb, J. E., Krotkov, N. A., Browell, E. V., Hair, J. W., Diskin, G., Sachse, G., and Vay, S. A.: In situ measurements of tropospheric volcanic plumes in Ecuador and Colombia during TC⁴, *J. Geophys. Res.-Atmos.*, 116, 1–24, <https://doi.org/10.1029/2010JD014718>, 2011.
- Chandler, A. S., Choulaton, T. W., Dollard, G. J., Eggleton, A. E. J., Gay, M. J., Hill, T. A., Jones, B. M. R., Tyler, B. J., Bandy, B. J., and Penkett, S. A.: Measurements of H₂O₂ and SO₂ in clouds and estimates of their reaction rate, *Nature*, 336, 562–565, <https://doi.org/10.1038/336562a0>, 1988.
- Chen, Q., Geng, L., Schmidt, J. A., Xie, Z., Kang, H., Dachs, J., Cole-Dai, J., Schauer, A. J., Camp, M. G., and Alexander, B.: Isotopic constraints on the role of hypohalous acids in sulfate aerosol formation in the remote marine boundary layer, *Atmos. Chem. Phys.*, 16, 11433–11450, <https://doi.org/10.5194/acp-16-11433-2016>, 2016.
- Chen, Q., Schmidt, J. A., Shah, V., Jaeglé, L., Sherwen, T., and Alexander, B.: Sulfate production by reactive bromine: Implications for the global sulfur and reactive bromine budgets, *Geophys. Res. Lett.*, 44, 7069–7078, <https://doi.org/10.1002/2017GL073812>, 2017.
- Chin, M. and Jacob, D. J.: Anthropogenic and natural contributions to tropospheric sulfate: A global model analysis, *J. Geophys. Res.-Atmos.*, 101, 18691–18699, <https://doi.org/10.1029/96JD01222>, 1996.
- Dahneke, B.: Simple Kinetic Theory of Brownian Diffusion in Vapors and Aerosols, in: *Theory Dispersed Multiph. Flow*, edited by: R.E. Meyer, 97–133, Elsevier, New York, <https://doi.org/10.1016/B978-0-12-493120-6.50011-8>, 1983.
- Daum, P. H., Kleinman, L. I., Hills, A. J., Lazrus, A. L., Leslie, A. C. D., Busness, K., and Boatman, J.: Measurement and Interpretation of Concentrations of H₂O₂ and Related Species in the Upper Midwest During Summer, 95, 9857–9871, <https://doi.org/10.1029/JD095iD07p09857>, 1990.
- De Moor, J. M., Fischer, T. P., Sharp, Z. D., King, P. L., Wilke, M., Botcharnikov, R. E., Cottrell, E., Zelenski, M., Marty, B., Klimm, K., Rivard, C., Ayalew, D., Ramirez, C., and Kelley, K. A.: Sulfur degassing at Erta Ale (Ethiopia) and Masaya (Nicaragua) volcanoes: Implications for degassing processes and oxygen fugacities of basaltic systems, *Geochemistry, Geophys. Geosystems*, 14, 4076–4108, <https://doi.org/10.1002/ggge.20255>, 2013.
- Delmelle, P.: Environmental impacts of tropospheric volcanic gas plumes, *Geol. Soc. London, Spec. Publ.*, 213, 381–399, <https://doi.org/10.1144/GSL.SP.2003.213.01.23>, 2003.
- Desboeufs, K. V., Losno, R., Vimeux, F., and Cholbi, S.: The pH-dependent dissolution of wind-transported Saharan dust, *J. Geophys. Res.-Atmos.*, 104, 21287–21299, <https://doi.org/10.1029/1999JD900236>, 1999.
- Desboeufs, K. V., Losno, R., and Colin, J. L.: Factors influencing aerosol solubility during cloud processes, *Atmos. Environ.*, 35, 3529–3537, [https://doi.org/10.1016/S1352-2310\(00\)00472-6](https://doi.org/10.1016/S1352-2310(00)00472-6), 2001.
- Dole, M.: The Relative Atomic Weight of Oxygen in Water and in Air A Discussion of the Atmospheric Distribution of the Oxygen Isotopes and of the Chemical Standard of Atomic Weights, *J. Chem. Phys.*, 4, 268, <https://doi.org/10.1063/1.1749834>, 1936.
- Dubey, M. K., Mohrschladt, R., Donahue, N. M., and Anderson, J. G.: Isotope Specific Kinetics of Hydroxyl Radical (OH) with Water (H₂O): Testing Models of Reactivity and Atmospheric Fractionation, *J. Phys. Chem. A*, 101, 1494–1500, <https://doi.org/10.1021/jp962332p>, 1997.
- Eiler, J. M.: Oxygen Isotope Variations of Basaltic Lavas and Upper Mantle Rocks, *Rev. Mineral. Geochemistry*, 43, 319–364, <https://doi.org/10.2138/gsrng.43.1.319>, 2001.
- Evans, M., Shallcross, D., Law, K., Wild, J., Simmonds, P., Spain, T., Berrisford, P., Methven, J., Lewis, A., McQuaid, J., Pilling, M., Bandy, B., Penkett, S., and Pyle, J.: Evaluation of a Lagrangian box model using field measurements from EASE (Eastern Atlantic Summer Experiment) 1996, *Atmos. Environ.*, 34, 3843–3863, [https://doi.org/10.1016/S1352-2310\(00\)00184-9](https://doi.org/10.1016/S1352-2310(00)00184-9), 2000.
- Gerlach, T. M.: Volcanic sources of tropospheric ozone-depleting trace gases, *Geochemistry, Geophys. Geosystems*, 5, <https://doi.org/10.1029/2004GC000747>, 2004.
- Gervat, G. P., Clark, P. A., Marsh, A. R. W., Teasdale, I., Chandler, A. S., Choulaton, T. W., Gay, M. J., Hill, M. K., and Hill, T. A.: Field evidence for the oxidation of SO₂ by H₂O₂ in cap clouds, *Nature*, 333, 241–243, <https://doi.org/10.1038/333241a0>, 1988.
- Goto, D., Nakajima, T., Takemura, T., and Sudo, K.: A study of uncertainties in the sulfate distribution and its radiative forcing associated with sulfur chemistry in a global aerosol model, *Atmos. Chem. Phys.*, 11, 10889–10910, <https://doi.org/10.5194/acp-11-10889-2011>, 2011.
- Graedel, T. E. and Weschler, C. J.: Chemistry within aqueous atmospheric aerosols and raindrops, 19, <https://doi.org/10.1029/RG019i004p00505>, 1981.
- Graf, H. F., Langmann, B., and Feichter, J.: The contribution of Earth degassing to the atmospheric sulfur budget, *Chem. Geol.*, 147, 131–145, [https://doi.org/10.1016/S0009-2541\(97\)00177-0](https://doi.org/10.1016/S0009-2541(97)00177-0), 1998.
- Gromov, S., Jöckel, P., Sander, R., and Brenninkmeijer, C. A. M.: A kinetic chemistry tagging technique and its application to modelling the stable isotopic composition of atmospheric trace gases, *Geosci. Model Dev.*, 3, 337–364, <https://doi.org/10.5194/gmd-3-337-2010>, 2010.
- Harris, E., Sinha, B., Hoppe, P., and Ono, S.: High-precision measurements of (³³S) and (³⁴S) fractionation during SO₂ oxidation reveal causes of seasonality in SO₂ and sulfate isotopic composition, *Environ. Sci. Technol.*, 47, 12174–12183, <https://doi.org/10.1021/es402824c>, 2013.

- Heidenreich III, J. E., Thiemens, M. H., Heidenreich, J. E., and Thiemens, M. H.: A non-mass-dependent oxygen isotope effect in the production of ozone from molecular oxygen: The role of molecular symmetry in isotope chemistry, *J. Chem. Phys.*, 84, 2129–2136, <https://doi.org/10.1063/1.450373>, 1986.
- Herrmann, H., Ervens, B., Jacobi, H. W., Wolke, R., Nowacki, P., and Zellner, R.: CAPRAM2.3: A chemical aqueous phase radical mechanism for tropospheric chemistry, *J. Atmos. Chem.*, 36, 231–284, <https://doi.org/10.1023/A:1006318622743>, 2000.
- Hoffmann, M. R.: On the kinetics and mechanism of oxidation of aquated sulfur dioxide by ozone, *Atmos. Environ.*, 20, 1145–1154, [https://doi.org/10.1016/0004-6981\(86\)90147-2](https://doi.org/10.1016/0004-6981(86)90147-2), 1986.
- Holt, B. D., Kumar, R., and Cunningham, P. T.: Oxygen-18 study of the aqueous-phase oxidation of sulfur dioxide, *Atmos. Environ.*, 15, 557–566, [https://doi.org/10.1016/0004-6981\(81\)90186-4](https://doi.org/10.1016/0004-6981(81)90186-4), 1981.
- Hoshyaripour, G., Hort, M., Langmann, B., and Delmelle, P.: Volcanic controls on ash iron solubility: New insights from high-temperature gas-ash interaction modeling, *J. Volcanol. Geotherm. Res.*, 286, 67–77, <https://doi.org/10.1016/j.jvolgeores.2014.09.005>, 2014.
- Hoshyaripour, G. A., Hort, M., and Langmann, B.: Ash iron mobilization through physicochemical processing in volcanic eruption plumes: a numerical modeling approach, *Atmos. Chem. Phys.*, 15, 9361–9379, <https://doi.org/10.5194/acp-15-9361-2015>, 2015.
- Ilyinskaya, E., Schmidt, A., Mather, T. A., Pope, F. D., Witham, C., Baxter, P., Jóhannsson, T., Pfeffer, M., Barsotti, S., Singh, A., Sanderson, P., Bergsson, B., McCormick Kilbride, B., Donovan, A., Peters, N., Oppenheimer, C., and Edmonds, M.: Understanding the environmental impacts of large fissure eruptions: Aerosol and gas emissions from the 2014–2015 Holuhraun eruption (Iceland), *Earth Planet. Sci. Lett.*, 472, 309–322, <https://doi.org/10.1016/j.epsl.2017.05.025>, 2017.
- Janssen, C.: Intramolecular isotope distribution in heavy ozone (¹⁶O¹⁸O¹⁶O and ¹⁶O¹⁶O¹⁸O), *J. Geophys. Res.-Atmos.*, 110, D08308, <https://doi.org/10.1029/2004JD005479>, 2005.
- Jeong, D., Kim, K., and Choi, W.: Accelerated dissolution of iron oxides in ice, *Atmos. Chem. Phys.*, 12, 11125–11133, <https://doi.org/10.5194/acp-12-11125-2012>, 2012.
- Johnston, J. C. and Thiemens, M. H.: The isotopic composition of tropospheric ozone in three environments, *J. Geophys. Res.-Atmos.*, 102, 25395–25404, <https://doi.org/10.1029/97JD02075>, 1997.
- Jourdain, L., Roberts, T. J., Pirre, M., and Josse, B.: Modeling the reactive halogen plume from Ambrym and its impact on the troposphere with the CCATT-BRAMS mesoscale model, *Atmos. Chem. Phys.*, 16, 12099–12125, <https://doi.org/10.5194/acp-16-12099-2016>, 2016.
- Korolev, A. V., Isaac, G. A., Strapp, J. W., Cober, S. G., and Barker, H. W.: In situ measurements of liquid water content profiles in midlatitude stratiform clouds, *Q. J. R. Meteorol. Soc.*, 133, 1693–1699, <https://doi.org/10.1002/qj.147>, 2007.
- Krankowsky, D., Bartecki, F., Klees, G. G., Mauersberger, K., Schellenbach, K., and Stehr, J.: Measurement of heavy isotope enrichment in tropospheric ozone, *Geophys. Res. Lett.*, 22, 1713–1716, <https://doi.org/10.1029/95GL01436>, 1995.
- Kristiansen, N. I., Stohl, A., Olivié, D. J. L., Croft, B., Søvde, O. A., Klein, H., Christoudias, T., Kunkel, D., Leadbetter, S. J., Lee, Y. H., Zhang, K., Tsigaridis, K., Bergman, T., Evangelio, N., Wang, H., Ma, P.-L., Easter, R. C., Rasch, P. J., Liu, X., Pitari, G., Di Genova, G., Zhao, S. Y., Balkanski, Y., Bauer, S. E., Faluvegi, G. S., Kokkola, H., Martin, R. V., Pierce, J. R., Schulz, M., Shindell, D., Tost, H., and Zhang, H.: Evaluation of observed and modelled aerosol lifetimes using radioactive tracers of opportunity and an ensemble of 19 global models, *Atmos. Chem. Phys.*, 16, 3525–3561, <https://doi.org/10.5194/acp-16-3525-2016>, 2016.
- Laj, P., Fuzzi, S., Facchini, M. C., Lind, J. A., Orsi, G., Preiss, M., Maser, R., Jaeschke, W., Seyffer, E., Helas, G., Acker, K., Wiedprecht, W., Moller, D., Arends, B. G., Mols, J. J., Colvile, R. N., Gallagher, M. W., Beswick, K. M., and Hargreaves, K. J.: Cloud processing of soluble gases, *Atmos. Environ.*, 31, 2589–2598, [https://doi.org/10.1016/S1352-2310\(97\)00040-X](https://doi.org/10.1016/S1352-2310(97)00040-X), 1997.
- Langmann, B.: On the role of climate forcing by volcanic sulphate and volcanic ash, *Adv. Meteorol.*, 2014, <https://doi.org/10.1155/2014/340123>, 2014.
- Lee, C. C.-W. and Thiemens, M. H.: The delta δ¹⁷O and δ¹⁸O measurements of atmospheric sulfate from a coastal and high alpine region: A mass-independent isotopic anomaly, *J. Geophys. Res.-Atmos.*, 106, 17359–17373, <https://doi.org/10.1029/2000JD900805>, 2001.
- Lee, C. C. W., Savarino, J., and Thiemens, M. H.: Mass independent oxygen isotopic composition of atmospheric sulfate: Origin and implications for the present and past atmosphere of Earth and Mars, *Geophys. Res. Lett.*, 28, 1783–1786, <https://doi.org/10.1029/2000GL011826>, 2001.
- Luz, B., Barkan, E., and Bender, M. L.: Triple-isotope composition of atmospheric oxygen as a tracer of biosphere productivity, *Nature*, 400, 547–550, <https://doi.org/10.1038/22987>, 1999.
- Lyons, J. R.: Transfer of mass-independent fractionation in ozone to other oxygen-containing radicals in the atmosphere, *Geophys. Res. Lett.*, 28, 3231–3234, <https://doi.org/10.1029/2000GL012791>, 2001.
- Marcus, R. A.: Theory of mass-independent fractionation of isotopes, phase space accessibility, and a role of isotopic symmetry, *Proc. Natl. Acad. Sci.*, 110, 17703–17707, <https://doi.org/10.1073/pnas.1213080110>, 2013.
- Martin, E.: Volcanic Plume Impact on the Atmosphere and Climate : O- and S-Isotope Insight into Sulfate Aerosol Formation, 1991, 1–23, <https://doi.org/10.3390/geosciences8060198>, 2018.
- Martin, E., Bekki, S., Ninin, C., and Bindeman, I.: Volcanic sulfate aerosol formation in the troposphere, *J. Geophys. Res.-Atmos.*, 119, 12660–12673, <https://doi.org/10.1002/2014JD021915>, 2014.
- Martin, L. and Good, T. W.: Catalyzed oxidation of sulfur dioxide in solution: The iron-manganese synergism, *Atmos. Environ. Part A. Gen. Top.*, 25, 2395–2399, [https://doi.org/10.1016/0960-1686\(91\)90113-L](https://doi.org/10.1016/0960-1686(91)90113-L), 1991.
- Martin, L. R.: Kinetic studies of sulfite oxidation in aqueous solution. In SO₂, NO and NO₂ Oxidation Mechanisms: Atmospheric Considerations, 63–100, 1984.
- Maters, E. C., Delmelle, P., and Bonneville, S.: Atmospheric Processing of Volcanic Glass: Effects on Iron Solubility and Redox Speciation, *Environ. Sci. Technol.*, 50, 5033–5040, <https://doi.org/10.1021/acs.est.5b06281>, 2016.
- Maters, E. C., Delmelle, P., and Gunnlaugsson, H. P.: Controls on iron mobilisation from volcanic ash at low pH: Insights from dis-

- solution experiments and Mössbauer spectroscopy, *Chem. Geol.*, 449, 73–81, <https://doi.org/10.1016/j.chemgeo.2016.11.036>, 2017.
- Mather, T., Pyle, D. M., and Oppenheimer, C.: Tropospheric volcanic aerosol, *Volcanism and the Earth's Atmosphere*, 189–212, <https://doi.org/10.1029/139GM12>, 2003.
- Mather, T. A., McCabe, J. R., Rai, V. K., Thiemens, M. H., Pyle, D. M., Heaton, T. H. E., Sloane, H. J., and Fern, G. R.: Oxygen and sulfur isotopic composition of volcanic sulfate aerosol at the point of emission, *J. Geophys. Res.-Atmos.*, 111, 1–9, <https://doi.org/10.1029/2005JD006584>, 2006.
- Mather, T. A., Witt, M. L., Pyle, D. M., Quayle, B. M., Aiuppa, A., Bagnato, E., Martin, R. S., Sims, K. W., Edmonds, M., Sutton, A. J., and Ilyinskaya, E.: Halogens and trace metal emissions from the ongoing 2008 summit eruption of Kilauea volcano, Hawai'i, *Geochim. Cosmochim. Ac.*, 83, 292–323, <https://doi.org/10.1016/j.gca.2011.11.029>, 2012.
- McArdle, J. V. and Hoffmann, M. R.: Kinetics and mechanism of the oxidation of aquated sulfur dioxide by hydrogen peroxide at low pH, *J. Phys. Chem.*, 87, 5425–5429, <https://doi.org/10.1021/j150644a024>, 1983.
- Methven, J., Arnold, S. R., Stohl, A., Evans, M. J., Avery, M., Law, K., Lewis, A. C., Monks, P. S., Parrish, D. D., Reeves, C. E., Schlager, H., Atlas, E. L., Blake, D. R., Coe, H., Crosier, J., Flocke, F. M., Holloway, J. S., Hopkins, J. R., McQuaid, J., Purvis, R., Rappenglück, B., Singh, H. B., Watson, N. M., Whalley, L. K., and Williams, P. I.: Establishing Lagrangian connections between observations within air masses crossing the Atlantic during the International Consortium for Atmospheric Research on Transport and Transformation experiment, *J. Geophys. Res.-Atmos.*, 111, 1–21, <https://doi.org/10.1029/2006JD007540>, 2006.
- Michalski, G. and Xu, F.: Isotope modeling of nitric acid formation in the atmosphere using ISO-RACM: testing the importance of NO oxidation, heterogeneous reactions, and trace gas chemistry, *Atmos. Chem. Phys. Discuss.*, 10, 6829–6869, <https://doi.org/10.5194/acpd-10-6829-2010>, 2010.
- Michalski, G., Scott, Z., Kabling, M., and Thiemens, M. H.: First measurements and modeling of $\Delta^{17}\text{O}$ in atmospheric nitrate, *Geophys. Res. Lett.*, 30, 1870, <https://doi.org/10.1029/2003GL017015>, 2003.
- Millard, G. A., Mather, T. A., Pyle, D. M., Rose, W. I., and Thornton, B.: Halogen emissions from a small volcanic eruption: Modeling the peak concentrations, dispersion, and volcanically induced ozone loss in the stratosphere, *Geophys. Res. Lett.*, 33, 6–11, <https://doi.org/10.1029/2006GL026959>, 2006.
- Miller, M. F.: Isotopic fractionation and the quantification of ^{17}O anomalies in the oxygen three-isotope system: An appraisal and geochemical significance, *Geochim. Cosmochim. Ac.*, 66, 1881–1889, [https://doi.org/10.1016/S0016-7037\(02\)00832-3](https://doi.org/10.1016/S0016-7037(02)00832-3), 2002.
- Morin, S., Savarino, J., Bekki, S., Gong, S., and Bottenheim, J. W.: Signature of Arctic surface ozone depletion events in the isotope anomaly ($\Delta^{17}\text{O}$) of atmospheric nitrate, *Atmos. Chem. Phys.*, 7, 1451–1469, <https://doi.org/10.5194/acp-7-1451-2007>, 2007.
- Morin, S., Savarino, J., Frey, M. M., Yan, N., Bekki, S., Bottenheim, J. W., and Martins, J. M. F.: Tracing the origin and fate of NO_x in the Arctic atmosphere using stable isotopes in nitrate., *Science*, 322, 730–732, <https://doi.org/10.1126/science.1161910>, 2008.
- Morin, S., Sander, R., and Savarino, J.: Simulation of the diurnal variations of the oxygen isotope anomaly ($\Delta^{17}\text{O}$) of reactive atmospheric species, *Atmos. Chem. Phys.*, 11, 3653–3671, <https://doi.org/10.5194/acp-11-3653-2011>, 2011.
- Oppenheimer, C., Fischer, T. P., and Scaillet, B.: Volcanic Degassing: Process and Impact, 4, 2013.
- Pack, A., Toulouse, C., and Przybilla, R.: Determination of oxygen triple isotope ratios of silicates without cryogenic separation of NF₃ – technique with application to analyses of technical O₂ gas and meteorite classification, *Rapid Commun. Mass Spectrom.*, 21, 3721–3728, <https://doi.org/10.1002/rcm.3269>, 2007.
- Parazols, M., Marinoni, A., Amato, P., Abida, O., Laj, P., and Mailhot, G.: Speciation and role of iron in cloud droplets at the puy de Dôme station, *J. Atmos. Chem.*, 54, 267–281, <https://doi.org/10.1007/s10874-006-9026-x>, 2006.
- Park, R. J., Jacob, D. J., Field, B. D., Yantosca, R. M., and Chin, M.: Natural and transboundary pollution influences on sulfate-nitrate-ammonium aerosols in the United States: Implications for policy, *J. Geophys. Res.-Atmos.*, 109, <https://doi.org/10.1029/2003JD004473>, 2004.
- Pope III, C. A.: Lung Cancer, Cardiopulmonary Mortality, and Long-term Exposure to Fine Particulate Air Pollution, *Jama*, 287, 1132, <https://doi.org/10.1001/jama.287.9.1132>, 2002.
- Pruppacher, H. R., Klett, J. D., and Wang, P. K.: Microphysics of Clouds and Precipitation, *Aerosol Sci. Technol.*, 28, 381–382, <https://doi.org/10.1080/02786829808965531>, 1998.
- Pugh, T. A. M., Cain, M., Methven, J., Wild, O., Arnold, S. R., Real, E., Law, K. S., Emmerson, K. M., Owen, S. M., Pyle, J. A., Hewitt, C. N., and MacKenzie, A. R.: A Lagrangian model of air-mass photochemistry and mixing using a trajectory ensemble: the Cambridge Tropospheric Trajectory model of Chemistry And Transport (CiTTyCAT) version 4.2, *Geosci. Model Dev.*, 5, 193–221, <https://doi.org/10.5194/gmd-5-193-2012>, 2012.
- Real, E., Law, K. S., Weinzierl, B., Fiebig, M., Petzold, A., Wild, O., Methven, J., Arnold, S., Stohl, A., Huntrieser, H., Roiger, A., Schlager, H., Stewart, D., Avery, M., Sachse, G., Browell, E., Ferrare, R., and Blake, D.: Processes influencing ozone levels in Alaskan forest fire plumes during long-range transport over the North Atlantic, *J. Geophys. Res.-Atmos.*, 112, D10S41, <https://doi.org/10.1029/2006JD007576>, 2007.
- Redlich, O.: The Dissociation of Strong Electrolytes., *Chem. Rev.*, 39, 333–356, <https://doi.org/10.1021/cr60123a005>, 1946.
- Ridley, D. A., Cain, M., Methven, J., and Arnold, S. R.: Sensitivity of tropospheric ozone to chemical kinetic uncertainties in air masses influenced by anthropogenic and biomass burning emissions, *Geophys. Res. Lett.*, 44, 7472–7481, <https://doi.org/10.1002/2017GL073802>, 2017.
- Roberts, T. J., Braban, C. F., Martin, R. S., Oppenheimer, C., Adams, J. W., Cox, R. A., Jones, R. L., and Griffiths, P. T.: Modelling reactive halogen formation and ozone depletion in volcanic plumes, *Chem. Geol.*, 263, 151–163, <https://doi.org/10.1016/j.chemgeo.2008.11.012>, 2009.
- Roberts, T. J., Braban, C. F., Oppenheimer, C., Martin, R. S., Freshwater, R. A., Dawson, D. H., Griffiths, P. T., Cox, R. A., Saffell, J. R., and Jones, R. L.: Electrochemical sensing of volcanic gases, *Chem. Geol.*, 332–333, 74–91, <https://doi.org/10.1016/j.chemgeo.2012.08.027>, 2012.
- Roberts, T. J., Martin, R. S., and Jourdain, L.: Reactive bromine chemistry in Mount Etna's volcanic plume: the influence of

- total Br, high-temperature processing, aerosol loading and plume-air mixing, *Atmos. Chem. Phys.*, 14, 11201–11219, <https://doi.org/10.5194/acp-14-11201-2014>, 2014.
- Robock, A.: Volcanic eruptions and climate, *Rev. Geophys.*, 38, 191–219, <https://doi.org/10.1029/1998RG000054>, 2000.
- Röckmann, T.: Mass-Independent Oxygen Isotope Fractionation in Atmospheric CO as a Result of the Reaction CO+OH, *Science*, 281, 544–546, <https://doi.org/10.1126/science.281.5376.544>, 1998.
- Rose, W. I. and Durant, A. J.: Fine ash content of explosive eruptions, *J. Volcanol. Geotherm. Res.*, 186, 32–39, <https://doi.org/10.1016/j.jvolgeores.2009.01.010>, 2009.
- Rose, W. I., Millard, G. A., Mather, T. A., Hunton, D. E., Anderson, B., Oppenheimer, C., Thornton, B. F., Gerlach, T. M., Viggiano, A. A., Kondo, Y., Miller, T. M., and Ballenthin, J. O.: Atmospheric chemistry of a 33–34 hour old volcanic cloud from Hekla Volcano (Iceland): Insights from direct sampling and the application of chemical box modeling, *J. Geophys. Res. Atmos.*, 111, 1–17, <https://doi.org/10.1029/2005JD006872>, 2006.
- Rosenfeld, D. and Lensky, I. M.: Satellite-Based Insights into Precipitation Formation Processes in Continental and Maritime Convective Clouds, *Bull. Am. Meteorol. Soc.*, 79, 2457–2476, [https://doi.org/10.1175/1520-0477\(1998\)079<2457:SBIIPF>2.0.CO;2](https://doi.org/10.1175/1520-0477(1998)079<2457:SBIIPF>2.0.CO;2), 1998.
- Sander, S. P., Friedl, R. R., Golden, D. M., Kurylo, M. J., Moortgat, G. K., Wine, P. H., Ravishankara, a. R., Kolb, C. E., Molina, M. J., Diego, S., Jolla, L., Huie, R. E., and Orkin, V. L.: Chemical Kinetics and Photochemical Data for Use in Atmospheric Studies Evaluation Number 15, Cross Sect., California, 1–153, <https://doi.org/10.1002/kin.550171010>, 2006.
- Savarino, J. and Thiemens, M. H.: Mass-independent oxygen isotope (¹⁶O, ¹⁷O, ¹⁸O) fractionation found in H_x, O_x reactions, *J. Phys. Chem. A*, 103, 9221–9229, <https://doi.org/10.1021/jp991221y>, 1999a.
- Savarino, J. and Thiemens, M. H.: Analytical procedure to determine both δ¹⁸O and δ¹⁷O of H₂O₂ in natural water and first measurements, *Atmos. Environ.*, 33, 3683–3690, [https://doi.org/10.1016/S1352-2310\(99\)00122-3](https://doi.org/10.1016/S1352-2310(99)00122-3), 1999b.
- Savarino, J., Lee, C. C. W., and Thiemens, M. H.: Laboratory oxygen isotopic study of sulfur (IV) oxidation: Origin of the mass-independent oxygen isotopic anomaly in atmospheric sulfates and sulfate mineral deposits on Earth, *J. Geophys. Res.-Atmos.*, 105, 29079–29088, <https://doi.org/10.1029/2000JD900456>, 2000.
- Savarino, J., Bekki, S., Cole-Dai, J., and Thiemens, M. H.: Evidence from sulfate mass independent oxygen isotopic compositions of dramatic changes in atmospheric oxidation following massive volcanic eruptions, *J. Geophys. Res.-Atmos.*, 108, 1–6, <https://doi.org/10.1029/2003JD003737>, 2003.
- Savarino, J., Kaiser, J., Morin, S., Sigman, D. M., and Thiemens, M. H.: Nitrogen and oxygen isotopic constraints on the origin of atmospheric nitrate in coastal Antarctica, *Atmos. Chem. Phys.*, 7, 1925–1945, <https://doi.org/10.5194/acp-7-1925-2007>, 2007.
- Savarino, J., Bhattacharya, S. K., Morin, S., Baroni, M., and Doussin, J.-F.: The NO+O₃ reaction: a triple oxygen isotope perspective on the reaction dynamics and atmospheric implications for the transfer of the ozone isotope anomaly., *J. Chem. Phys.*, 128, 194303, <https://doi.org/10.1063/1.2917581>, 2008.
- Seinfeld, J. H. and Pandis, S. N.: Atmospheric chemistry and physics: from air pollution to climate change, 3 Edn., <https://doi.org/10.1021/ja985605y>, 2016.
- Sheppard, M. G. and Walker, R. B.: Wigner method studies of ozone photodissociation, *J. Chem. Phys.*, 78, 7191–7199, <https://doi.org/10.1063/1.444760>, 1983.
- Shi, Z., Krom, M. D., Jickells, T. D., Bonneville, S., Carslaw, K. S., Mihalopoulos, N., Baker, A. R., and Benning, L. G.: Impacts on iron solubility in the mineral dust by processes in the source region and the atmosphere: A review, *Aeolian Res.*, 5, 21–42, <https://doi.org/10.1016/j.aeolia.2012.03.001>, 2012.
- Smith, S. J., van Aardenne, J., Klimont, Z., Andres, R. J., Volke, A., and Delgado Arias, S.: Anthropogenic sulfur dioxide emissions: 1850–2005, *Atmos. Chem. Phys.*, 11, 1101–1116, <https://doi.org/10.5194/acp-11-1101-2011>, 2011.
- Solmon, F., Chuang, P. Y., Meskhidze, N., and Chen, Y.: Acidic processing of mineral dust iron by anthropogenic compounds over the north Pacific Ocean, *J. Geophys. Res.-Atmos.*, 114, 1–20, <https://doi.org/10.1029/2008JD010417>, 2009.
- Stefánsson, A., Stefánssdóttir, G., Keller, N. S., Barsotti, S., Sigurdsson, Á., Thorláksdóttir, S. B., Pfeffer, M. A., Eiríksdóttir, E. S., Jónasdóttir, E. B., von Löwis, S., and Gíslason, S. R.: Major impact of volcanic gases on the chemical composition of precipitation in Iceland during the 2014–2015 Holuhraun eruption, *J. Geophys. Res.-Atmos.*, 122, 1971–1982, <https://doi.org/10.1002/2015JD024093>, 2017.
- Stevenson, D. S., Johnson, C. E., Collins, W. J., and Derwent, R. G.: The tropospheric sulphur cycle and the role of volcanic SO₂, *Geol. Soc. London, Spec. Publ.*, 213, 295–305, <https://doi.org/10.1144/GSL.SP.2003.213.01.18>, 2003a.
- Highwood, E.-J. and Stevenson, D. S.: Atmospheric impact of the 1783–1784 Laki Eruption: Part II Climatic effect of sulphate aerosol, *Atmos. Chem. Phys.*, 3, 1177–1189, <https://doi.org/10.5194/acp-3-1177-2003>, 2003b.
- Stocker, T., Qin, D., Plattner, G.-K., Tignor, M., Allen, S., Boschung, J., Nauels, A., Xia, Y., Bex, V., Midgley, P., et al.: Climate Change 2013: The Physical Science Basis. Contribution of Working Group I to the Fifth Assessment Report of the Intergovernmental Panel on Climate Change, 5th, Cambridge University Press, Cambridge, United Kingdom and New York, NY, USA, <https://doi.org/10.1017/CBO9781107415324>, 2013.
- Tabazadeh, A. and Turco, R. P.: Stratospheric Chlorine Injection by Volcanic Eruptions: HCI Scavenging and Implications for Ozone, *Science*, 260, 1082–1086, <https://doi.org/10.1126/science.260.5111.1082>, 1993.
- Textor, C., Graf, H.-F., Timmreck, C., and Robock, A.: Emissions from volcanoes, in: *Emiss. Atmos. trace Compd.*, 269–303, 2004.
- Thiemens, M. H.: History and applications of mass-independent isotope effects, *Annu. Rev. Earth Planet. Sci.*, 34, 217–262, <https://doi.org/10.1146/annurev.earth.34.031405.125026>, 2006.
- Thomason, L. and Peter, T., ed.: SPARC Assessment of Stratospheric Aerosol Properties (ASAP), SPARC Office, no. 4 Edn., available at: <http://www.sparc-climate.org/publications/sparc-reports/> (last access: February 2016), 2006.
- Uemura, R., Barkan, E., Abe, O., and Luz, B.: Triple isotope composition of oxygen in atmospheric water vapor, *Geophys. Res. Lett.*, 37, L04402, <https://doi.org/10.1029/2009GL041960>, 2010.
- Vicars, W. C. and Savarino, J.: Quantitative constraints on the ¹⁷O-excess (Δ¹⁷O) signature of surface ozone: Ambient

- measurements from 50° N to 50° S using the nitrite-coated filter technique, *Geochim. Cosmochim. Ac.*, 135, 270–287, <https://doi.org/10.1016/j.gca.2014.03.023>, 2014.
- Vogt, R., Crutzen, P. J., and Sander, R.: A mechanism for halogen release from sea-salt aerosol in the remote marine boundary layer, 383, 327–330, <https://doi.org/10.1038/383327a0>, 1996.
- Voigt, C., Jessberger, P., Jurkat, T., Kaufmann, S., Baumann, R., Schlager, H., Bobrowski, N., Giuffrida, G., and Salerno, G.: Evolution of CO₂, SO₂, HCl, and HNO₃ in the volcanic plumes from Etna, *Geophys. Res. Lett.*, 41, 2196–2203, <https://doi.org/10.1002/2013GL058974>, 2014.
- von Glasow, R.: Atmospheric chemistry in volcanic plumes, *Proc. Natl. Acad. Sci.*, 107, 6594–6599, <https://doi.org/10.1073/pnas.0913164107>, 2010.
- von Glasow, R. and Crutzen, P. J.: Tropospheric Halogen Chemistry, *Treatise Geochemistry Second Ed.*, 5, 19–69, <https://doi.org/10.1016/B978-0-08-095975-7.00402-2>, 2013.
- von Glasow, R., Sander, R., Bott, A., and Crutzen, P. J.: Modeling halogen chemistry in the marine boundary layer 2. Interactions with sulfur and the cloud-covered MBL, *J. Geophys. Res.-Atmos.*, 107, 1–13, <https://doi.org/10.1029/2001JD000943>, 2002.
- Wardell, L. J., Kyle, P. R., and Chaffin, C.: Carbon dioxide and carbon monoxide emission rates from an alkaline intra-plate volcano: Mt. Erebus, Antarctica, *J. Volcanol. Geotherm. Res.*, 131, 109–121, [https://doi.org/10.1016/S0377-0273\(03\)00320-2](https://doi.org/10.1016/S0377-0273(03)00320-2), 2004.
- Wild, O., Zhu, X., and Prather, M. J.: Fast-J: Accurate simulation of in- and below-cloud photolysis in tropospheric chemical models, *J. Atmos. Chem.*, 37, 245–282, <https://doi.org/10.1023/A:1006415919030>, 2000.
- World Health Organization: The European Health Report 2009 – Health and health systems, 1–191, 2009.
- Young, E. D., Galy, A., and Nagahara, H.: Kinetic and equilibrium mass-dependant isotope fractionation laws in nature and their geochemical and cosmochemical significance, *Geochim. Cosmochim. Ac.*, 66, 1095–1104, [https://doi.org/10.1016/S0016-7037\(01\)00832-8](https://doi.org/10.1016/S0016-7037(01)00832-8), 2002.
- Young, E. D., Yeung, L. Y., and Kohl, I. E.: On the δ¹⁷O budget of atmospheric O₂, *Geochim. Cosmochim. Ac.*, 135, 102–125, <https://doi.org/10.1016/j.gca.2014.03.026>, 2014.
- Zuo, Y. and Hoigne, J.: Evidence for Photochemical Formation of H₂O₂ and Oxidation of SO₂ in Authentic Fog Water, *Science*, 260, 71–73, <https://doi.org/10.1126/science.260.5104.71>, 1993.